Numerical Approximation of the Nonlinear Shallow Water Equations with Topography and Dry Beds: A Godunov-Type Scheme

David L. George

A thesis submitted in partial fulfillment of the requirements for the degree of

Master of Science

University of Washington

2004

Program Authorized to Offer Degree: Applied Mathematics

TABLE OF CONTENTS

LIST OF FIGURES

Chapter 1

BACKGROUND

1.1 Introduction

The flow of water over a surface is a ubiquitous physical phenomenon of practical interest to many scientists and engineers. For instance, flows such as ocean tides, wind waves, dam breaches, river floods, and tsunamis support a large interest from diverse fields for diverse reasons. Despite the everyday familiarity of water flow, the governing equations for the internal flow comprise an intractable set of equations, too complex to be of practical use for most applications. Accordingly, approximate descriptions of the flow are often of more use, assuming the approximation is acceptable for the particular application. An approximation of common use for many applications leads to the *shallow water equations*—a system of nonlinear partial differential equations approximating the surface and horizontal momentum of the flow. Although simplified from the complete governing equations, the shallow water equations can nonetheless rarely be exactly solved and even present many difficulties for numerical computation. Furthermore, many real applications introduce further complications, such as variable topography and evolving dry regions within the domain. Recently much progress has been made using Godunov-type finite volume methods for the shallow water equations (see for example [2, 7, 12, 1]), however no single numerical method is without weakness and few, if any, are reliable for all types of shallow flows.

A robust numerical method that can reliably and accurately solve the shallow water equations over variable topography in diverse conditions is sought. Here I present a high-resolution Godunov-type finite volume method with a novel Riemann solver that has some

promising features for the one-dimensional case, and ultimately might be the basis for a two-dimensional high-resolution method.

1.2   Derivation of the Shallow Water Equations

The applications mentioned above are described by a subset of fluid dynamical theory, in which an incompressible fluid under gravity has a free surface at an unknown location. Further, the viscosity of the fluid is usually ignored as it is negligible relative to the large scales of these flows. The nonlinear shallow water equations arise when some additional assumptions about the flow are included; several equivalent assumptions lead to the same set of equations. Most formally, starting with the full three dimensional equations describing an inviscid and incompressible fluid, the shallow water equations are the lowest order approximation when a perturbation procedure is developed for all quantities. In this perturbation procedure, the parameter ϵ, which is the ratio of the water depth to some characteristic horizontal length of the flow, is assumed to be small. This procedure results in the vertical acceleration of water particles that is zero (to lowest order), which is equivalent to a vertically hydrostatic pressure distribution. The most straight-forward derivation of the shallow water equations, and the one shown below, comes from starting with this hydrostatic assumption *a priori*. Adding this assumption to the inviscid and incompressible assumptions, the shallow water equations follow immediately from conservation of mass and momentum. Variable bottom topography contributes a source of momentum. See [16] or [19] for a more complete description of the shallow water assumptions.

Consider an incompressible fluid of depth h over a bottom surface $z = b(x, y)$, with a velocity field $\mathbf{u} = [u, v, w]$. See Figure 1.1. It can be shown that $\mathbf{u}$ is independent of z since the pressure gradient is independent of z. For conservation of momentum we start with an arbitrary region Ω^3, in three dimensions, with the bottom surface $b(x, y)$ and free surface $h(x, y)$ defining the top and bottom boundaries. Conservation of momentum in this region
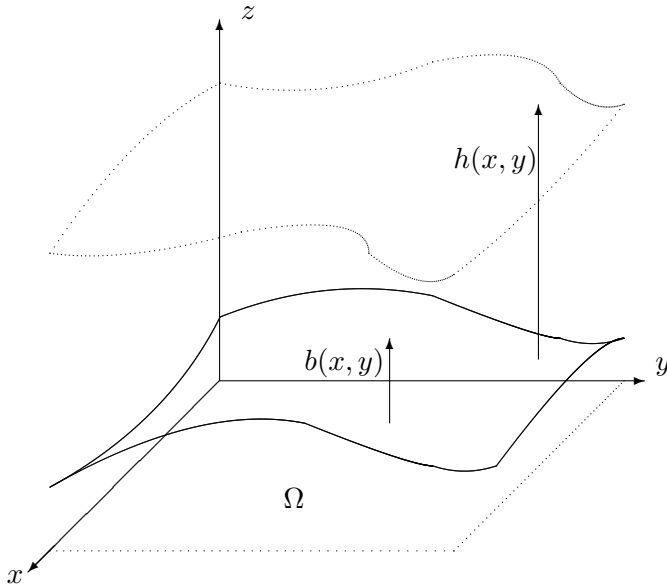
Figure 1.1: Depiction of the variables for the shallow water equations. For the full two-dimensional shallow water equations, surfaces depend on x and y. The lower surface is the bottom b, with the water of depth h over it.

gives[1]

$$\frac{d}{dt} \iiint_{\Omega^3} \mathbf{u} \, dx \, dy \, dz + \iint_{\partial\Omega^3} [(\mathbf{u})\mathbf{u} \cdot \mathbf{n}] \, ds + \iint_{\partial\Omega^3} [\Pi \cdot \mathbf{n}] \, ds - \iiint_{\Omega^3} \mathbf{G} \, dx \, dy \, dz = 0, \quad (1.1)$$

where the second integral on the left is the flux of momentum due to advection across the boundaries, Π is the stress tensor and $\mathbf{G}$ is the body force density, $-g\hat{\mathbf{k}}$. Assuming an inviscid fluid gives a stress tensor with merely the hydrostatic pressure, $p(x, y, z) = g(h+b-z)$ on the diagonal, $\Pi = p\mathbf{I}$. Because of the hydrostatic assumption, the vertical component of the last two integrals of course cancels. The the third equation for w in (1.1) is therefore neglected, since it asserts that $Dw/Dt = 0$. Integrating the pressure at the top $(p(x, y, h) = 0)$ and bottom $(p(x, y, b) = gh)$ surfaces, and integrating out the vertical coordinate, leads to

$$\frac{d}{dt} \iint_{\Omega} h\mathbf{u} \, dx \, dy + \int_{\partial\Omega} [(h\mathbf{u})\mathbf{u} \cdot \mathbf{n}] \, ds + \int_{\partial\Omega} \left[\frac{1}{2}gh^2\mathbf{n}\right] ds = -\iint_{\Omega} gh\nabla b \, dx \, dy. \quad (1.2)$$

---

[1] The constant density has been dropped from all equations.

The third integral is due to pressure at the boundaries of the two-dimensional region Ω, after the vertical coordinate has been integrated. The term on the right is a source of momentum due to variable bottom topography, and comes from integrating the pressure at the bottom. Conservation of mass over an arbitrary fixed region Ω in the x–y plane comes from considering the two-dimensional velocity field $\mathbf{u} = [u, v]$

$$\frac{d}{dt} \iint_\Omega h \, dx \, dy + \int_{\partial\Omega} h\mathbf{u} \cdot \mathbf{n} \, ds = 0, \tag{1.3}$$

where the second integral on the left is the flux of mass into the region due to flow crossing the boundaries.

Conservation of mass, equation (1.3), and the two conservation of momentum equations in (1.2) together comprise the set of governing equations for the depth and momentum of the flow. This set of equations belongs to a broader class of conservation laws, which can be compactly written as

$$\frac{d}{dt} \iint_\Omega \mathbf{q} \, dx \, dy + \int_{\partial\Omega} F(\mathbf{q}) \cdot \mathbf{n} \, ds = \iint_\Omega \psi \, dx \, dy, \tag{1.4}$$

where for the shallow water equations,

$$\mathbf{q} = \begin{bmatrix} h \\ hu \\ hv \end{bmatrix}, \quad F = \begin{bmatrix} hu & hv \\ hu^2 + \frac{1}{2}gh^2 & huv \\ huv & hv^2 + \frac{1}{2}gh^2 \end{bmatrix}, \quad \psi = \begin{bmatrix} 0 \\ -ghb_x \\ -ghb_y \end{bmatrix}.$$

The system (1.4) is the integral form of the conservation laws, and is more fundamental than further manipulated forms of the system.[2] This integral form admits discontinuous solutions provided that they satisfy certain conditions at the discontinuity; see Section 1.3. Manipulation of the integral form into a system of PDEs requires continuity of the solution, and is therefore not always valid. A numerical method based on the conservative integral form is therefore preferable to one based solely on the derived PDEs. However, deriving the PDE form is helpful for theoretical reasons and is shown below.

---

[2]Conservation laws modified by a source term are often called "balance laws," yet here I will continue to refer to them as "conservation laws," it being understood that the source term contributes to the quantity normally conserved.

Applying the divergence theorem to the second integral in (1.4) and moving the time derivative into the first integral, assuming that the solution is continuous and differentiable, results in the following system:

$$\iint_\Omega \mathbf{q}_t \, dx \, dy + \iint_\Omega [\mathbf{f}(\mathbf{q})_x + \mathbf{g}(\mathbf{q})_y] \, dx \, dy = \iint_\Omega \psi \, dx \, dy \qquad (1.5)$$

where the flux components $\mathbf{f}$ and $\mathbf{g}$ are the first and second columns of $\mathbf{F}$, respectively. The arbitrariness of the domain Ω implies the following system of PDEs:

$$\mathbf{q}_t + \mathbf{f}(\mathbf{q})_x + \mathbf{g}(\mathbf{q})_y = \psi. \qquad (1.6)$$

Taking the derivatives of $\mathbf{f}$ and $\mathbf{g}$, again assuming that the solution is continuous and differentiable, results in the quasi-linear system

$$\mathbf{q}_t + \mathbf{f}'(\mathbf{q})\mathbf{q}_x + \mathbf{g}'(\mathbf{q})\mathbf{q}_y = \psi \qquad (1.7)$$

where $\mathbf{f}'(\mathbf{q})$ and $\mathbf{g}'(\mathbf{q})$ are the Jacobian matrices of the functions $\mathbf{f}$ and $\mathbf{g}$. A conservation law such as (1.7) is hyperbolic if every linear combination of $\mathbf{f}'(\mathbf{q})$ and $\mathbf{g}'(\mathbf{q})$ has real eigenvalues, and can be diagonalized. The shallow water equations are hyperbolic conservation laws.

In this thesis I present a method for the one-dimensional shallow water equations, where the integral and PDE form of the conservation laws become respectively

$$\frac{d}{dt} \int_{x_1}^{x_2} \mathbf{q}(x, t) \, dx + \mathbf{f}(\mathbf{q}(x_2, t)) - \mathbf{f}(\mathbf{q}(x_1, t)) = \int_{x_1}^{x_2} \psi \, dx \qquad (1.8)$$

and

$$\mathbf{q}_t + \mathbf{f}(\mathbf{q})_x = \psi. \qquad (1.9)$$

As in two dimensions, if the solution is continuous and differentiable, equation (1.9) is equivalent to

$$\mathbf{q}_t + \mathbf{f}'(\mathbf{q})\mathbf{q}_x = \psi. \qquad (1.10)$$

The system (1.10) is hyperbolic if $\mathbf{f}'(\mathbf{q})$ has real eigenvalues and is diagonalizable. For the shallow water equations

$$\mathbf{q} = \begin{bmatrix} h \\ hu \end{bmatrix}, \quad \mathbf{f} = \begin{bmatrix} hu \\ hu^2 + \frac{1}{2}gh^2 \end{bmatrix}, \quad \psi = \begin{bmatrix} 0 \\ -ghb_x \end{bmatrix},$$

so when put in the form of (1.10) the one-dimensional shallow water equations become

$$
\begin{bmatrix} h \\ hu \end{bmatrix}_t + \begin{bmatrix} 0 & 1 \\ -u^2 + gh & 2u \end{bmatrix} \begin{bmatrix} h \\ hu \end{bmatrix}_x = \begin{bmatrix} 0 \\ -ghb_x \end{bmatrix}. \tag{1.11}
$$

The system (1.11) is hyperbolic since the Jacobian matrix

$$
\mathbf{f}'(\mathbf{q}) = \begin{bmatrix} 0 & 1 \\ -u^2 + gh & 2u \end{bmatrix}
$$

has eigenvalues $\lambda^1 = u - \sqrt{gh}$ and $\lambda^2 = u + \sqrt{gh}$. These values are obviously real and distinct as long as h is positive.

For hyperbolic systems such as (1.10) information travels from one point to another at speeds equal to the eigenvalues of the Jacobian matrix. For reasons that will become clear below, these eigenvalues are sometimes called "characteristic speeds" and curves in space-time upon which the information travels are sometimes called "characteristic curves." For a system of n equations there are n eigenvalues, and hence n families of characteristic curves. If the eigenvalues are distinct, the n curves are never parallel at a given point in the space-time plane. For a more complete discussion of the properties of hyperbolic systems see for example [15] or [8].

1.3 Discontinuities and the Rankine-Hugoniot Condition

The more fundamental integral form of conservation laws (1.8) admits discontinuous solutions or "shocks."[3] In manipulating the integral conservation laws into the PDEs, smoothness of the solution was assumed. Since the PDEs contain derivatives that are undefined at a discontinuity, a solution must always satisfy the more fundamental integral form across a discontinuity. Consider a propagating jump discontinuity moving at speed s. By applying

---

[3]The term "shock" is borrowed from gas dynamics, where the physical manifestation of a mathematical discontinuity is a shock-wave. In shallow water theory a discontinuity is usually referred to as a "bore," however, to maintain consistent terminology for equivalent mathematical properties, I will use the term shock throughout.
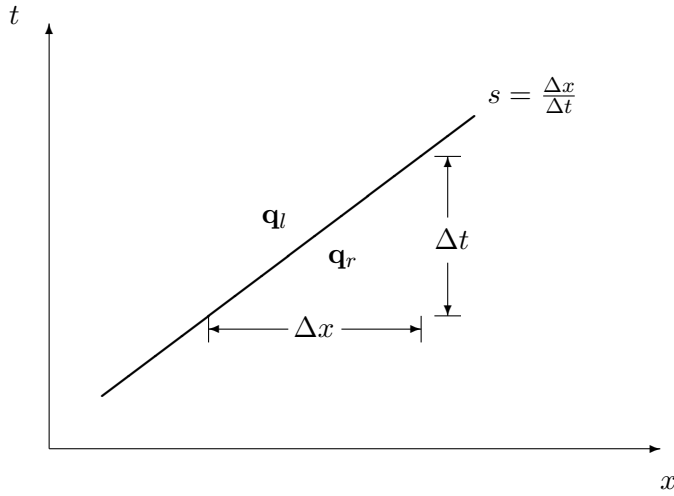
Figure 1.2: Depiction of a shock moving at speed s with states $\mathbf{q}_l$ and $\mathbf{q}_r$ immediately to the left and right of the shock respectively. To satisfy the Rankine-Hugoniot jump condition the following relation must hold: $s\left(\mathbf{q}_r - \mathbf{q}_l\right) = \mathbf{f}(\mathbf{q}_r) - \mathbf{f}(\mathbf{q}_l)$.

(1.8) to an arbitrarily small region surrounding the discontinuity, it is easy to show that the discontinuity must satisfy the following condition known as the Rankine-Hugoniot condition

$$s\left(\mathbf{q}_r - \mathbf{q}_l\right) = \mathbf{f}(\mathbf{q}_r) - \mathbf{f}(\mathbf{q}_l), \tag{1.12}$$

where $\mathbf{q}_r$ and $\mathbf{q}_l$ are the solutions immediately to the right and left of the discontinuity respectively; see Figure 1.2. A solution that satisfies the integral conservation laws, and hence the PDEs where smooth, and satisfies the Rankine-Hugoniot condition across a discontinuity is known as a "weak solution" to the conservation laws; see [15].

By allowing discontinuous solutions subject to (1.12), uniqueness of a weak solution is not always guaranteed and often other admissibility conditions must be imposed based on physical considerations above and beyond the conservation laws. These additional constraints often take the form of an "entropy" function that is conserved except across a discontinuity; see [15].

1.4 Conservative Finite Volume Methods

From a numerical viewpoint, shock waves pose a difficulty that precludes the use of many methods. Use of a naive method can lead to spurious oscillations near a shock wave, computing shocks with the wrong strength, or propagating shocks with the wrong speed; see [15] or [18]. The numerical method proposed in this paper is based on the type of finite volume methods developed in [15]. These methods are particularly suited for dealing with hyperbolic systems that allow various discontinuities such as shocks in the weak solution, and were largely developed for the Euler equations of gas dynamics—a hyperbolic system with many similarities to the shallow water equations. With a finite volume approach, the numerical solution approximates the average value of the solution in each discrete computational cell. Consider the integral form of the conservation laws (1.8), neglecting the source term temporarily,

$$\frac{d}{dt}\int_{x_1}^{x_2} \mathbf{q}(x,t)\,dx\,dy = -\left[\mathbf{f}(\mathbf{q}(x_2,t)) - \mathbf{f}(\mathbf{q}(x_1,t))\right]. \tag{1.13}$$

Applying (1.13) exactly over a computational cell $\Omega_i = \left[x_{i-\frac{1}{2}}, x_{i+\frac{1}{2}}\right]$,

$$\frac{d}{dt}\int_{\Omega_i} \mathbf{q}(x,t)\,dx = -\left[\mathbf{f}(\mathbf{q}(x_{i+\frac{1}{2}},t)) - \mathbf{f}(\mathbf{q}(x_{i-\frac{1}{2}},t))\right]$$

and integrating over a time interval $\tau^n = \left[t^n, t^{n+1}\right]$, gives

$$\int_{\Omega_i} \mathbf{q}(x,t^{n+1})\,dx = \int_{\Omega_i} \mathbf{q}(x,t^n)\,dx - \int_{\tau^n}\left[\mathbf{f}(\mathbf{q}(x_{i+\frac{1}{2}},t)) - \mathbf{f}(\mathbf{q}(x_{i-\frac{1}{2}},t))\right]\,dt.$$

This system can be rewritten as

$$\mathbf{Q}_i^{n+1} = \mathbf{Q}_i^n - \frac{\Delta t}{\Delta x}\left[\mathbf{F}_{i+\frac{1}{2}}^n - \mathbf{F}_{i-\frac{1}{2}}^n\right] \tag{1.14}$$

where $\mathbf{Q}_i$ is the spatial average of $\mathbf{q}$ over the cell Ω_i

$$\mathbf{Q}_i = \frac{1}{\Delta x}\int_{\Omega_i} \mathbf{q}(x,t)\,dx \tag{1.15}$$

and $\mathbf{F}_{i\pm\frac{1}{2}}^n$ are the time-averaged fluxes at the boundaries over a time-step τ^n

$$\mathbf{F}_{i\pm\frac{1}{2}}^n = \frac{1}{\Delta t}\int_{\tau^n} \mathbf{f}(\mathbf{q}(x_{i\pm\frac{1}{2}})). \tag{1.16}$$

Equation (1.14) is exactly met by the true solution over a time interval if $\mathbf{F}^n_{i\pm\frac{1}{2}}$ are the true time averaged fluxes at the boundaries. Additionally (1.14) is the basis of conservative finite volume methods for (1.13), where $\mathbf{F}^n_{i\pm\frac{1}{2}}$ are numerical fluxes—approximations to the true time-averaged fluxes at the cell boundaries.

Equation (1.14) is a conservative numerical method since it conserves the numerical variable $\mathbf{Q}_i$ on the computing domain (aside from any input or output at the boundaries). When numerically approximating integral conservation laws with discontinuous weak solutions, a conservative method based on the integral conservation laws can converge properly to a discontinuous weak solution, where a method based on the PDEs alone often fails to converge to a correct weak solution. In fact, Hou and LeFloch [11] proved that if a non-conservative method is used, it converges to the wrong solution if it contains a shock wave. For a more complete discussion of pathological behavior of nonconservative methods, and the convergence of conservative methods to the right weak solution, see [15] or [18].

1.5 Godunov's Method and the Riemann Problem

Developing a conservative flux-differencing method based on (1.14) essentially amounts to establishing a proper estimate for the time averaged fluxes (1.16). The method developed in this paper is a Godunov-type method—a class of numerical methods that have proven to be successful at dealing with many of the difficulties of hyperbolic conservation laws, such as shocks. Godunov-type methods are upwind methods where a Riemann problem

$$\mathbf{q}_t + \mathbf{f}'(\mathbf{q})\mathbf{q}_x = 0$$
$$\mathbf{q}(x,0) = \begin{cases} \mathbf{q}_l & x < 0 \\ \mathbf{q}_r & x > 0 \end{cases} \tag{1.17}$$

is solved at each cell interface before each time-step. The relevance of the Riemann problems can be seen from considering the solution to be a piecewise constant function with the cell average value $\mathbf{Q}_i$, throughout each cell. At the cell interfaces $x_{i-\frac{1}{2}}$, there are discontinuities with $\mathbf{q}_l = \mathbf{Q}_{i-1}$ to the left and $\mathbf{q}_r = \mathbf{Q}_i$ to the right. In Godunov's method the numerical

fluxes used in (1.14) come from evaluating the true flux function with the solution from the Riemann problem (1.17) at each cell interface

$$\mathbf{Q}_i^{n+1} = \mathbf{Q}_i^n - \frac{\Delta t}{\Delta x}\left[\mathbf{f}(\mathbf{q}_{i+\frac{1}{2}}^n) - \mathbf{f}(\mathbf{q}_{i-\frac{1}{2}}^n)\right] \tag{1.18}$$

where $\mathbf{q}_{i\pm\frac{1}{2}}^n$ are the solutions to the Riemann problems at $x_{i\pm\frac{1}{2}}$ given initial data

$$\mathbf{q}(x,t^n) = \begin{cases} \mathbf{Q}_{i-1}^n & x < x_{i-\frac{1}{2}} \\ \mathbf{Q}_i^n & x > x_{i-\frac{1}{2}}. \end{cases} \tag{1.19}$$

At the end of a time-step the data is re-averaged and the process is begun again. By using Riemann solutions, Godunov's method has a proper upwind bias, even when characteristic information moves in both directions. For a first-order accurate method, this upwind bias is necessary for stability; see [15] or [17].

For many systems, such as the shallow water equations, an exact solution to the Riemann problem (1.17) is a similarity solution depending on x and t only as a single variable x/t. That is, the solution to the Riemann problem, $\mathbf{q}(x,t)$ is of the form $\tilde{\mathbf{q}}(x/t)$. The particular values of x/t are of course rays in the space-time plane connected at the initial discontinuity at $x = 0$. I will refer to this spreading region in the x–t plane as the "Riemann solution." At a given time, to the far right and far left of the Riemann solution, the solution is still constant and the same as the initial conditions since the characteristic information from the initial discontinuity has not had time to reach these regions. Since the characteristic curves for each family must be unique at any point in space-time, the characteristic speeds in the Riemann solution either make a smooth transition into the characteristic speeds outside the Riemann solution, or are separated by a shock from the speeds outside the solution. This set of transitions can be viewed as waves emanating from the initial discontinuity, as the solution only varies across each transition. For the shallow water equations there are two characteristic families, and hence two such transitions or waves. A smooth transition occurs when the speeds of a characteristic family increase from left to right, and is known as a "rarefaction" as it usually corresponds to a solution that is rarefied, or less dense, behind the wave. If the speeds of a characteristic family decrease from left to right, the regions are
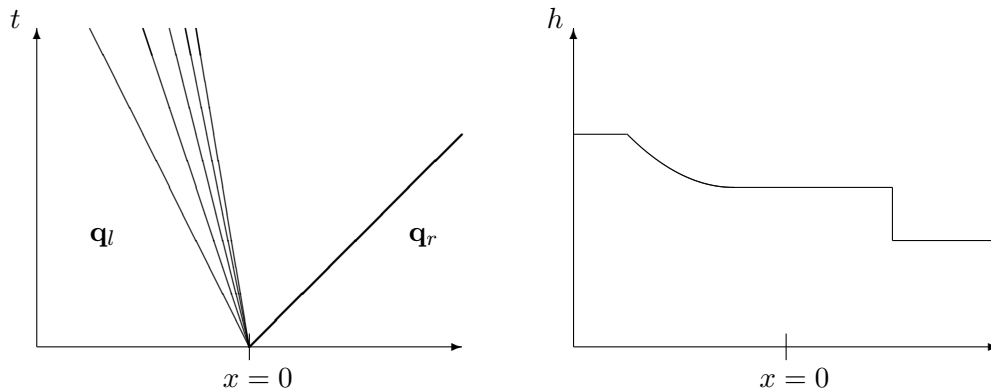
Figure 1.3: An example of a Riemann solution to the shallow water equations with a rarefaction in the first characteristic family and a shock in the second family. Left: Characteristic transitions, or waves emanating from the initial discontinuity are shown in the x–t plane. Right: The first component of the solution, the water depth h, is shown at some time after $t = 0$

separated by a shock. A Riemann solution may be composed of any combination of shocks or rarefactions in the particular characteristic families, depending on the particular initial data.[4] Figure 1.3 is an example of a Riemann solution to the shallow water equations, with a shock in one characteristic family and a rarefaction in the other.

For the homogeneous shallow water equations, the Riemann problems can be solved exactly, yet at a considerable expense due to the nonlinear flux function; see [15]. Furthermore, the entire Riemann solution is not even needed, just the constant value at the cell interface, $x/t = 0$. Therefore, it is often preferable to use an approximate Riemann solution.

1.6   Linear Problems

Approximate solutions to Riemann problems are often based on solutions to a linear Riemann problem, that is, (1.17) with a linear flux function $\mathbf{f}(\mathbf{q}) = \mathbf{A}\mathbf{q}$. Consider a hyperbolic

---

[4]A full discussion of exact solutions to Riemann problems and how to construct such solutions is beyond the scope of this thesis, but can be found in [15],[17].

system with such a flux function:

$$\mathbf{q}_t + \mathbf{A}\mathbf{q}_x = 0. \tag{1.20}$$

In order to be hyperbolic, $\mathbf{A}$ must have distinct real eigenvalues and can therefore be diagonalized: $\mathbf{A} = \mathbf{R}\mathbf{\Lambda}\mathbf{R}^{-1}$, where $\mathbf{\Lambda}$ is the diagonal matrix of eigenvalues, and $\mathbf{R}$ is the matrix of right eigenvectors. Substituting $\mathbf{A} = \mathbf{R}\mathbf{\Lambda}\mathbf{R}^{-1}$ in (1.20) and multiplying by $\mathbf{R}^{-1}$ gives [5]

$$\mathbf{w}_t + \mathbf{\Lambda}\mathbf{w}_x = 0 \tag{1.21}$$

where $\mathbf{w}$ is the vector of characteristic variables

$$\mathbf{w} = \mathbf{R}^{-1}\mathbf{q}, \qquad \mathbf{w} = [\begin{array}{ccc} w^1 & \cdots & w^n \end{array}]^T.$$

Because of the diagonal matrix, equation (1.21) is a system of n decoupled scalar advection equations

$$w_t^p + \lambda^p w_x^p = 0, \qquad p = 1, \dots, n \ . \tag{1.22}$$

Therefore, the initial profile of each characteristic variable w^p simply advects at its characteristic speed—the corresponding eigenvalue λ^p. Converting back to the original variables shows that the solution consists of a weighted superposition of the eigenvectors of $\mathbf{A}$, where the profile of each weight advects at the speed of the corresponding eigenvalue, or

$$\mathbf{q} = \mathbf{R}\mathbf{w} \qquad \text{where} \qquad w^p(x,t) = w^p(x - \lambda^p t, 0), \qquad p = 1, \dots, n. \tag{1.23}$$

Now consider a Riemann problem with (1.20), where initially there is a single discontinuity,

$$\mathbf{q}_t + \mathbf{A}\mathbf{q}_x = 0$$
$$\mathbf{q}(x,0) = \begin{cases} \mathbf{q}_l & x < 0 \\ \mathbf{q}_r & x > 0. \end{cases} \tag{1.24}$$

Considering (1.23), it can be seen that the solution to (1.24) is a piecewise constant with discontinuities spreading out from the initial interface at the speeds of the eigenvalues. The

---

[5]This requires $\mathbf{R}$ to be constant since therefore $\mathbf{R}^{-1}\mathbf{q}_t = \left(\mathbf{R}^{-1}\mathbf{q}\right)_t = \mathbf{w}_t$.
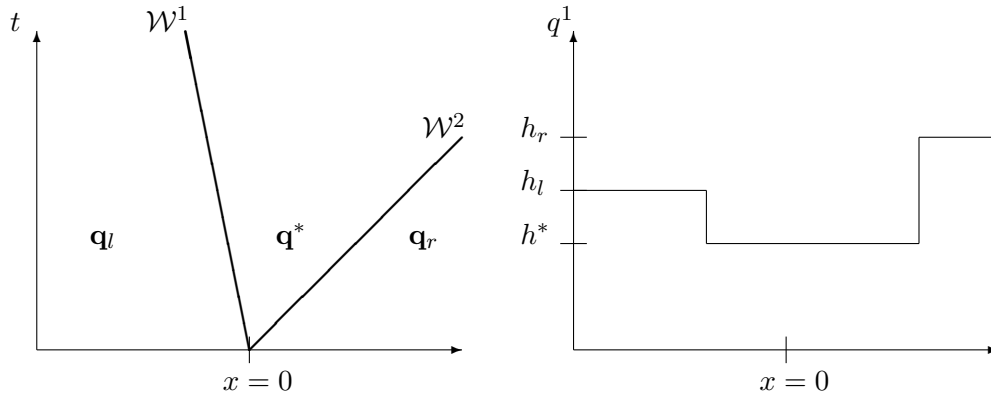
Figure 1.4: An example of a linear Riemann solution to a system of two equations. Left: Depiction of the linear Riemann solution in the x–t plane. Right: Example of the first component of the solution, denoted $q^1 = h$, shown at some time after $t = 0$.

jump across the pth discontinuity (a vector with n components) will be denoted $\mathcal{W}^p$. It can also be seen by considering (1.23) that the jump across each propagating discontinuity is proportional to the corresponding eigenvector

$$\mathcal{W}^p = (w_r^p - w_l^p)\mathbf{r}^p = \alpha^p \mathbf{r}^p \tag{1.25}$$

where $\mathbf{r}^p$ is the pth eigenvector of $\mathbf{A}$ or p^{th} column of $\mathbf{R}$. Note that these discontinuities automatically satisfy the Rankine-Hugoniot condition (1.12), which when applied to a linear flux function simply requires a discontinuity to be an eigenvector of $\mathbf{A}$ propagating at a speed s equal to the corresponding eigenvalue, λ^p.

If there are two equations in the system (1.20), then a linear Riemann solution has three states: the original state to the left, $\mathbf{q}_l$, the original state to the right, $\mathbf{q}_r$, and a middle state between the two discontinuities or waves, $\mathcal{W}^1$ and $\mathcal{W}^2$. This middle state will be denoted with a star: $\mathbf{q}^*$. See Figure 1.4, which illustrates a typical linear Riemann solution to a system of two equations.

1.7   The Roe Approximate Riemann Solver

One method for approximately solving a nonlinear Riemann problem (1.17) is to simply replace the nonlinear Jacobian matrix $\mathbf{f}'(\mathbf{q})$ with a diagonalizable constant matrix, so that the solution is equivalent to (1.23). Given different Riemann problems at each cell interface, it seems logical to base the constant matrix on the local data for each Riemann problem. Furthermore, evaluating $\mathbf{f}'(\mathbf{q})$ at some value, say $\hat{\mathbf{q}}$, based on $\mathbf{Q}_{i-1} = \mathbf{q}_l$ and $\mathbf{Q}_i = \mathbf{q}_r$ will preserve the eigenstructure of $\mathbf{f}'(\mathbf{q})$ and hence will be diagonalizable

$$\hat{\mathbf{A}}(\mathbf{q}_l, \mathbf{q}_r) = \mathbf{f}'\left(\hat{\mathbf{q}}(\mathbf{q}_l, \mathbf{q}_r)\right). \tag{1.26}$$

In the event that the exact solution to the Riemann problem consists of a single shock, we might require the linear solution to match the exact solution. This requirement is satisfied if the following condition on $\hat{\mathbf{A}}(\mathbf{q}_l, \mathbf{q}_r)$ is imposed:

$$\hat{\mathbf{A}}(\mathbf{q}_r - \mathbf{q}_l) = \mathbf{f}(\mathbf{q}_r) - \mathbf{f}(\mathbf{q}_l) \tag{1.27}$$

for arbitrary $\mathbf{q}_l$ and $\mathbf{q}_r$. The matrix $\hat{\mathbf{A}}$ then has an eigenstructure that gives the exact solution in the event of a single shock. This can be seen by recalling the Rankine-Hugoniot condition (1.12), which must be satisfied by the single shock

$$\mathbf{f}(\mathbf{q}_r) - \mathbf{f}(\mathbf{q}_l) = s(\mathbf{q}_r - \mathbf{q}_l). \tag{1.28}$$

Together (1.27) applied at a cell interface and (1.28) lead to

$$\hat{\mathbf{A}}(\mathbf{q}_r - \mathbf{q}_l) = \mathbf{f}(\mathbf{q}_r) - \mathbf{f}(\mathbf{q}_l) = s(\mathbf{q}_r - \mathbf{q}_l) \tag{1.29}$$

implying that the single shock is an eigenvector of $\hat{\mathbf{A}}$. The intermediate value $\hat{\mathbf{q}}$ in (1.26) such that (1.27) is satisfied, is known as the Roe average and $\hat{\mathbf{A}} = \mathbf{f}'(\hat{\mathbf{q}})$ the Roe matrix. For the one-dimensional shallow water equations

$$\hat{\mathbf{q}} = \left[\begin{array}{c} \hat{h} \\ \hat{h}\hat{u} \end{array} \right]$$

where

$$\hat{h} = \frac{h_l + h_r}{2}, \qquad \text{and} \qquad \hat{u} = \frac{u_l \sqrt{h_l} + u_r \sqrt{h_r}}{\sqrt{h_l} + \sqrt{h_r}}.$$

The motivation for the properties of the Roe matrix come from the fact that for a typical application the solution is likely smooth in the majority of the domain, or if a discontinuity exists it is most likely a single shock. Therefore, when a solution is discretized the adjacent cells in smooth regions have data that is nearly continuous, [6] and cells next to a single shock when discretized generate a Riemann problem with nearly a single shock solution; see [15].

1.8 Dry States and Failure of the Roe Solver

The Roe solver works well for many shallow water flows but in certain situations can produce negative depths. In addition to being obviously physically incorrect, these negative depths usually crash the computation. Consider the solution to a linear Riemann problem (1.24) with a Roe matrix $\hat{\mathbf{A}}$. The solution's middle state, $\mathbf{q}^*$, is connected to the state on the left, $\mathbf{q}_l$, by a jump in the first eigenvector of $\hat{\mathbf{A}}$ and is connected to the state on the right, $\mathbf{q}_r$, by a jump in the second eigenvector. The left and right states are therefore joined in phase space by the two eigenvectors, the middle state, $\mathbf{q}^*$, being the intersection of the two vectors. This intersection corresponds to a negative depth when the left and right states lay in particular regions of phase space; see Figure 1.5. For instance, if the velocity on the right is much greater than the velocity on the left and the flow is already very shallow, the intersection often corresponds to a negative depth. For applications where the flow is very shallow in parts of the domain, or in fact becomes dry in regions, the Roe solver is almost certain to produce negative depths. One way around this difficulty is to compute the exact Riemann solution, which as mentioned is possible for the homogeneous shallow water equations. However, this is computationally expensive, and it is not clear how to extend this satisfactorily to a Riemann problem with a source term.

---

[6]In regions with at least one continuous derivative, if the grid spacing is Δx, then $||\mathbf{Q}_i - \mathbf{Q}_{i-1}|| = \mathcal{O}(\Delta x)$
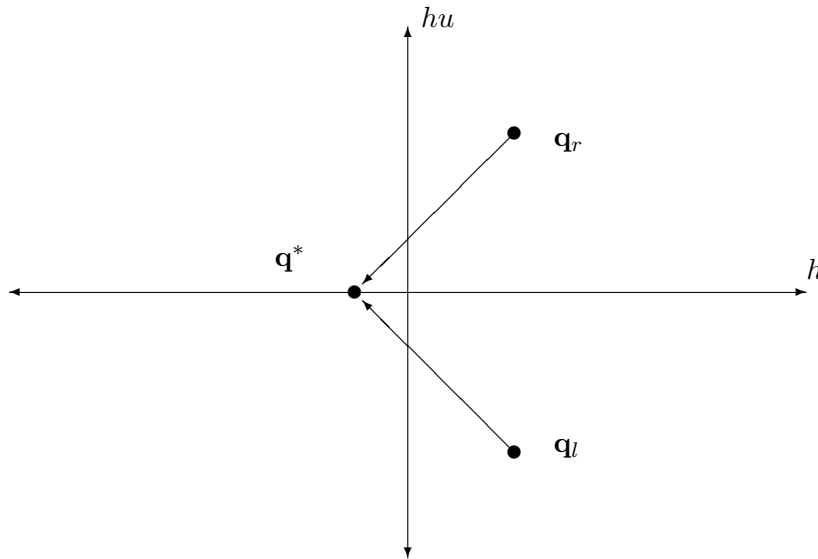
Figure 1.5: Failure of the Roe solver when the left and right states, $\mathbf{q}_l$ and $\mathbf{q}_r$, lay in particular regions of phase space. In this example the left and right states are shallow, with opposite velocities. The arrows are in the direction of the Roe eigenvectors, the intersection of which is the middle state $\mathbf{q}^*$, corresponding to a negative depth h.

1.9 The HLL Approximate Riemann Solvers

The HLL Riemann solvers are another class of linear approximation methods, originally developed for the Euler equations of gas dynamics, that are easily extended to the homogeneous shallow water equations; see [10]. These solvers are based on estimating the speeds that information or waves propagate away from a Riemann problem. A linear solution with two discontinuities is then constructed[7], using estimates for the speeds of the propagating discontinuities.[8] The estimates for the speeds are based on the initial data, and general properties of exact Riemann solutions. A number of different estimates for the speeds have been used, and the particular choice of estimates gives an HLL method its particular

[7]Two speeds are used in the original HLL method even for equations with more than two characteristic families.

[8]Contrast this to a method such as the Roe solver, where a constant estimate to the Jacobian matrix is constructed first, and the eigenvalues of this estimate subsequently affect the approximate Riemann solution.
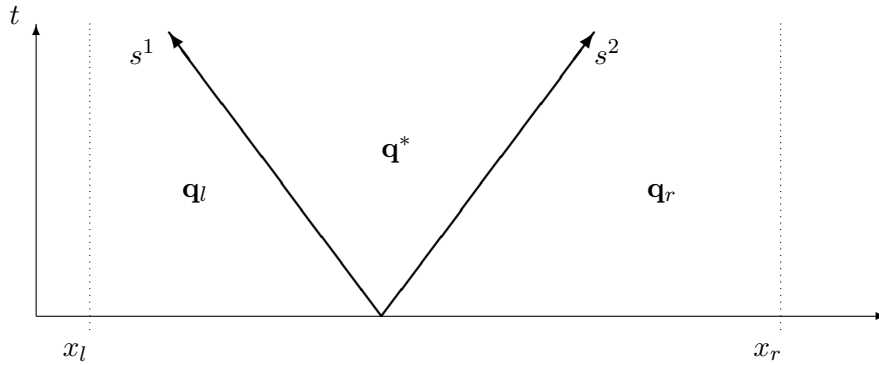
Figure 1.6: Constructing a solution using conservation and estimated speeds. If the speeds s^1 and s^2 are predetermined estimates, an approximate solution can be uniquely determined by applying the conservation law to the region $\Omega = [x_l, x_r]$ surrounding the interface.

properties; see [17].

Once estimates of the speeds are established, the approximate Riemann solution is constructed based on applying the original integral form of the conservation laws (1.13) to a region surrounding the Riemann solution. Imagine evaluating the flux function at two points, x_l and x_r, to the far left and far right of the Riemann solution. The Riemann solution is approximated as a piecewise constant solution with two discontinuities spreading out with the estimated speeds s^1 and s^2; see Figure 1.6. The value of the middle solution, $\mathbf{q}^*$ can be determined uniquely (neglecting the source term for now) from (1.13), which when applied to the region gives

$$
\begin{aligned}
\frac{d}{dt} \int_{x_l}^{x_r} \mathbf{q}(x,t)\, dx &= -\left[\mathbf{f}(\mathbf{q}(x_r,t)) - \mathbf{f}(\mathbf{q}(x_l,t))\right] \\
\Rightarrow -s^2 \left(\mathbf{q}_r - \mathbf{q}^*\right) - s^1 \left(\mathbf{q}^* - \mathbf{q}_l\right) &= -\left[\mathbf{f}(\mathbf{q}(x_r,t)) - \mathbf{f}(\mathbf{q}(x_l,t))\right].
\end{aligned}
\tag{1.30}
$$

Solving for the middle state $\mathbf{q}^*$ in (1.30), assuming $s^2 - s^1$ is greater than zero, gives

$$
\mathbf{q}^* = \left(\frac{1}{s^2 - s^1}\right) \left(\mathbf{f}(\mathbf{q}_l) - \mathbf{f}(\mathbf{q}_r) - s^1 \mathbf{q}_l + s^2 \mathbf{q}_r\right).
\tag{1.31}
$$

Note that (1.31) is two equations, one for each component of $\mathbf{q}^*$.

18

Riemann solutions of this form are conservative, in the sense that the structure of the approximate Riemann solution obeys the original conservation laws (1.13) when applied to the region surrounding the Riemann solution. This is not necessarily the case with any approximate Riemann solution, even if the overall numerical method is conservative. For instance, if the numerical method is based on using interface fluxes as in (1.14), the numerical solution is conserved overall even if the interface fluxes are based on Riemann solutions that are not conservative. However, if the numerical updating is based on using the actual structure of the solutions to the Riemann problems, rather than using interface fluxes as in (1.14), then the Riemann solutions must be conservative in order for the overall method to be conservative.[9] For a discussion of "wave-propagation" methods that use the structure of the Riemann solution for updating, see [15].

1.10 Source Terms from Topography

In most real applications there is variable bottom topography that adds a source term to the shallow water equations. All of the solutions discussed so far have dealt with homogeneous equations of the form (1.13), rather than the full form with a source term

$$\mathbf{q}_t + \mathbf{f}(\mathbf{q})_x = \psi. \tag{1.32}$$

A standard and easy way to deal with a source term is to treat it independently by using a fractional step method. That is, alternate between two problems

$$\mathbf{q}_t + \mathbf{f}(\mathbf{q})_x = 0 \tag{1.33}$$

$$\mathbf{q}_t = \psi. \tag{1.34}$$

First, problem (1.33) is solved and the solution is advanced partially, followed by problem (1.34) in each time-step. With this technique the homogeneous equation can be solved by

---

[9]The requirement (1.27) on the Roe matrix has an added benefit to that discussed in Section 1.7—it ensures that the structure of the solution is conservative.

any traditional method, and the source term merely adds the need for a step with any appropriate numerical method for a system of ordinary differential equations.[10]

One drawback of fractional step methods is their inability to preserve certain steady-states; see [14]. A common situation in applications involving the shallow water equations is the physically trivial situation of undisturbed motionless water over topography, time independent steady-flows, or perhaps small perturbations from such situations. Numerically, such situations are not so trivial, and the numerical preservation of such steady-states is a very desirable property in any numerical method for the shallow water equations; see [9]. The failure of fractional step methods in such situations can be foreseen by considering nearly time independent flow of any kind, where the flux gradient and source terms must approximately balance

$$\mathbf{q}_t + \mathbf{f}(\mathbf{q})_x = \psi$$
$$\mathbf{q}_t \approx 0$$
$$\Rightarrow \mathbf{f}(\mathbf{q})_x \approx \psi.$$

Given steep topography, the source term and flux gradient can be quite large, and each fraction of the update in (1.33) and (1.34) must undo the other in order to preserve the balance. Clearly this is not the best way to preserve steady-states or resolve small perturbations from steady-states, since preserving a delicate balance requires precise cancellation.

The method proposed in [1] circumvents this problem by taking advantage of the balance between the source and flux gradient. Recall that with a linear Riemann solution, such as that obtained when using a local approximation to the Jacobian such as a Roe matrix $\hat{\mathbf{A}}$, the jump initially at the cell interface, $\mathbf{q}_r - \mathbf{q}_l = \mathbf{Q}_i - \mathbf{Q}_{i-1}$, is broken up into the eigenvectors of $\hat{\mathbf{A}}$

$$\mathbf{q}_r - \mathbf{q}_l = \alpha^1 \hat{\mathbf{r}}^1 + \alpha^2 \hat{\mathbf{r}}^2 \tag{1.35}$$

---

[10]By using a fractional step method the problem of negative states mentioned in Section (1.8) can be circumvented by using the exact Riemann solution, however the expense of the exact Riemann solution remains as a deterrent, as well as the drawbacks of fractional step methods in general.

where $\hat{\mathbf{r}}^p$ are the eigenvectors and α^p are scalar multiples. Given a Roe matrix, the flux difference at a cell interface $\mathbf{f}(\mathbf{q}_r) - \mathbf{f}(\mathbf{q}_l)$ satisfies (1.27), which together with (1.35) implies

$$\mathbf{f}(\mathbf{q}_r) - \mathbf{f}(\mathbf{q}_l) = \hat{\mathbf{A}}\,(\mathbf{q}_r - \mathbf{q}_l) = \hat{\lambda}^1 \alpha^1 \hat{\mathbf{r}}^1 + \hat{\lambda}^1 \alpha^2 \hat{\mathbf{r}}^2 \tag{1.36}$$

where $\hat{\lambda}^p$ are the eigenvalues corresponding to $\hat{\mathbf{r}}^p$. Note from (1.36) that the flux difference at a cell interface is ultimately decomposed into the eigenvectors of the Roe matrix $\hat{\mathbf{A}}$[11]

$$\mathbf{f}(\mathbf{q}_r) - \mathbf{f}(\mathbf{q}_l) = \beta^1 \hat{\mathbf{r}}^1 + \beta^2 \hat{\mathbf{r}}^2. \tag{1.37}$$

In the wave propagation algorithms described in [15], the structure of the Riemann solution arising from a cell interface is used to update or re-average the solution. Considering the structure of linear solutions discussed in Section 1.6, the right hand side of equation (1.36) represents the propagation of discontinuities $\alpha^p \mathbf{r}^p$ propagating at speeds λ^p, and it is this structure that can be used to update the solution. Therefore, ultimately the right hand side of equation (1.37), the decomposition of the flux difference, can be used to update the solution. In [1] it is proposed that, when there is a source term, the flux difference minus the source term should be projected onto the eigenvectors arising from the Riemann problem and subsequently used to update the solution

$$\mathbf{f}(\mathbf{q}_r) - \mathbf{f}(\mathbf{q}_l) - \psi \Delta x = \beta^1 \hat{\mathbf{r}}^1 + \beta^2 \hat{\mathbf{r}}^2. \tag{1.38}$$

By using (1.38) it is the *difference* in the flux gradient and source that is used to update the solution, so that if the flux gradient and source term nearly balance—the situation for a steady-state—the updating will be small and the steady-state preserved.

Unfortunately the method described above does not circumvent the difficulty encountered with near dry states.

---

[11]The same conclusion can be reached more generally for other types of linear methods that do not necessarily use a Roe matrix. In the wave propagation formulation used in [15] the discontinuities arising from an interface can be viewed as waves spreading out from an interface. If these waves and their travelling speeds are used as a basis for updating the average in a cell, conservation dictates that the jump in flux must be the sum of these waves multiplied by the speeds. The flux difference is therefore decomposed into a linear combination of these waves, equivalent to (1.36); see [15] for a detailed discussion.

Chapter 2

A HIGH-RESOLUTION GODUNOV-TYPE SCHEME FOR THE SHALLOW WATER EQUATIONS

2.1 Desirable Properties

The utility of a numerical method for the shallow water equations depends on its ability to deal with various difficulties arising simultaneously in applications. Since the shallow water equations admit shocks, a method should be able to accurately capture moving jump discontinuities. Many applications have realistic arbitrary topography and regions of the domain that are sometimes dry and sometimes wet, so a method should be robust enough to deal with the appearance, or preexistence, of dry-states while at the same time handle a reasonably wide range of bottom topographies. For instance, it should be able to accurately resolve water advancing onto dry topography. Furthermore, it should be able to preserve steady-states as well as resolve small perturbations from steady-states, even when adjacent to dry regions.

In this chapter a high-resolution Godunov-type scheme is developed. It has given satisfactory results for the above conditions in one dimension. Like other Godunov-type schemes it can accurately capture moving shocks, and avoids spurious oscillations near those shocks. Moving dry-states within the computing domain are captured without the appearance of negative-states. The method maintains important steady-states, such as the physically trivial situation of a motionless pool of water over variable and steep topography, even when surrounded by dry regions.

2.2 A Positive-Depth Preserving Approximate Riemann Solver for the Homogeneous Shallow Water Equations

The problem of negative depths in approximate Riemann solutions mentioned in Section 1.8 must be overcome if a method is to handle very shallow flows with moving dry regions in the domain. The exact Riemann solution is one way to circumvent this problem, but even aside from its computational expense, it is not clear how to incorporate the source term into such a solution. There are so-called "positivity-preserving" approximate Riemann solutions that are based on an extension to the original HLL method discussed in Section 1.9. These were originally developed for gas dynamics, where near vacuum densities create an analogous problem to that of near dry-states in the shallow water equations. One such method is the HLLE method, where the estimates for the two speeds used in (1.31) are particular estimates for the maximum possible characteristic or shock speeds arising from a Riemann problem; see [5] or [6]. The estimates are based on the general structure of exact Riemann solutions discussed in Section 1.5. In an exact Riemann solution to systems such as the Euler and shallow water equations, a shock in a characteristic family occurs when the characteristic speed is less to the right of the shock than the left. The opposite is true in the case of a rarefaction. Based on these facts the estimates used in the HLLE method are

$$ s^1 \;\; = \;\; \min_p \left(\min \left(\lambda_l^p, \hat{\lambda}^p \right) \right) \tag{2.1} $$

$$ s^2 \;\; = \;\; \max_p \left(\max \left(\lambda_r^p, \hat{\lambda}^p \right) \right) \tag{2.2} $$

where λ^p is the pth eigenvalue to the left or right, and $\hat{\lambda}^p$ are the eigenvalues of the Roe matrix $\hat{\mathbf{A}}$ from the interface. The eigenvalues of the Roe matrix serve as estimates of the shock speeds arising from the Riemann problem, and the other values are the true maximum characteristic speeds in the case of rarefactions.

The relevance of the maximum speeds when trying to preserve positivity is elucidated in the following intuitive argument: regardless of the structure of the Riemann solution, the total change in mass in the region is determined by the flux at the two far boundaries where the solution is constant; see (1.30). If the flux-difference is large and positive, there

will be a large rate of decrease in mass in the region between the spreading discontinuities. The further this region spreads in a given amount of time, the less concentrated the given decrease in the solution is, and the less likely the solution will become negative in this region. It can be shown that by using proper estimates for the maximum speeds, such as (2.1) and (2.2), the solution in the middle region, $\mathbf{q}^*$, will always be non-negative. This is formulated as a theorem for emphasis.

Theorem 1. *For the homogeneous shallow water equations—equation (1.11) with no source term—if the middle state $\mathbf{q}^*$ is determined from (1.31), using (2.1) and (2.2) for the speeds s^1 and s^2, the depth h^* in the middle state is always non-negative.*

Proof: For the shallow water equations, the speeds (2.1) and (2.2) are equivalent to

$$s^1 = \min\left(u_l - \sqrt{gh_l}, \hat{u} - \sqrt{g\hat{h}}\right) \tag{2.3}$$

$$s^2 = \max\left(u_r + \sqrt{gh_r}, \hat{u} + \sqrt{g\hat{h}}\right) \tag{2.4}$$

where the Roe averages $\hat{u}$ and $\hat{h}$ are defined in Section 1.7. The first equation in (1.31) for the depth h^* of the middle state gives

$$h^* = \frac{h_l u_l - h_r u_r + s^2 h_r - s^1 h_l}{s^2 - s^1}. \tag{2.5}$$

Inserting (2.3) and (2.4) into (2.5) gives

$$h^* = \frac{h_l u_l - h_r u_r + \max\left(u_r + \sqrt{gh_r}, \hat{u} + \sqrt{g\hat{h}}\right) h_r - \min\left(u_l - \sqrt{gh_l}, \hat{u} - \sqrt{g\hat{h}}\right) h_l}{\max\left(u_r + \sqrt{gh_r}, \hat{u} + \sqrt{g\hat{h}}\right) - \min\left(u_l - \sqrt{gh_l}, \hat{u} - \sqrt{g\hat{h}}\right)}. \tag{2.6}$$

The denominator of (2.6) is always positive in regions with water:

$$
\begin{aligned}
& \max\left(u_r + \sqrt{gh_r}, \hat{u} + \sqrt{g\hat{h}}\right) - \min\left(u_l - \sqrt{gh_l}, \hat{u} - \sqrt{g\hat{h}}\right) \\
\geq\ & \left(\hat{u} + \sqrt{g\hat{h}}\right) - \left(\hat{u} - \sqrt{g\hat{h}}\right) \\
=\ & 2\sqrt{g\hat{h}} \\
>\ & 0.
\end{aligned}
\tag{2.7}
$$

And the numerator is always non-negative

$$
\begin{aligned}
& h_l u_l - h_r u_r + \max\left(u_r + \sqrt{gh_r}, \hat{u} + \sqrt{g\hat{h}}\right) h_r - \min\left(u_l - \sqrt{gh_l}, \hat{u} - \sqrt{g\hat{h}}\right) h_l \\
\geq\; & h_l u_l - h_r u_r + \left(u_r + \sqrt{gh_r}\right) h_r - \left(u_l - \sqrt{gh_l}\right) h_l \\
=\; & h_r \sqrt{gh_r} + h_l \sqrt{gh_l} \\
\geq\; & 0.
\end{aligned}
\tag{2.8}
$$

These results are for the homogeneous shallow water equations. How the HLLE method has been extended for the inclusion of a source term is described in the following sections.

2.3 Treatment of the Source Term

Because of the problems associated with a fractional step method described in Section 1.10, the method developed and described in this chapter incorporates the source term from topography directly into the Riemann problem. That is, the actual approximate Riemann solution includes the effect of a source term, and the updating of the solution is based solely on the structure of the solution.

Recall that the source term in the shallow water equations (1.11) arises from the derivative of the bottom elevation b,

$$
\psi = \begin{bmatrix} 0 \\ -ghb_x \end{bmatrix}.
\tag{2.9}
$$

Given a piecewise discretization of the bottom topography b_i, constant over each cell interval $\Omega_i = \left[x_{i-\frac{1}{2}}, x_{i+\frac{1}{2}}\right]$

$$
b_i = b(x_i)
\tag{2.10}
$$

the idealized source formally becomes a delta function at each cell interface

$$
\psi(x) \to \sum_i \mathbf{\Psi}_{i-\frac{1}{2}} \delta\left(x - x_{i-\frac{1}{2}}\right), \qquad \mathbf{\Psi}_{i-\frac{1}{2}} = \begin{bmatrix} 0 \\ -g\bar{h}_{i-\frac{1}{2}}(b_i - b_{i-1}) \end{bmatrix}.
\tag{2.11}
$$

Several options are available for the depth $\bar{h}_{i-\frac{1}{2}}$, used in (2.11) to approximate h in (2.9). To avoid the problem of overlapping discontinuities, the source term can be treated explicitly

in the sense that the value $\bar{h}_{i-\frac{1}{2}}$ is determined from the starting values before the Riemann problem is solved. For instance it can be taken to be the arithmetic average of the depth to the right and left of the interface $x_{i-\frac{1}{2}}$ before each time-step, $\bar{h}_{i-\frac{1}{2}} = \frac{1}{2}(h_i + h_{i-1})$. This is the approach used in the method developed in this section. However, it could be treated implicitly in that an average based on the solution to the Riemann problem is used.

A delta function source (2.11) might presumably lead to a discontinuity in the solution. To investigate how such a source might affect a solution, consider a stationary source at a cell interface, $\boldsymbol{\Psi}\delta(x - x_{i-\frac{1}{2}})$. By applying the conservation law (1.8) to an arbitrarily small interval surrounding the source, the following jump condition can be shown:

$$\mathbf{f}(\mathbf{q}_r^*) - \mathbf{f}(\mathbf{q}_l^*) = \Psi \tag{2.12}$$

where $\mathbf{q}_l^*$ and $\mathbf{q}_r^*$ represent the solution to the right and left of the source respectively. The result (2.12) is valid if the source itself is not a function of the solution, which is discontinuous at the source, creating a problem for the theory of distributions as it involves overlapping discontinuities; see [4].

If the source term is treated explicitly, Ψ depends on constant values determined before the start of the Riemann problem

$$\boldsymbol{\Psi}_{i-\frac{1}{2}} = \begin{bmatrix} 0 \\ -g\bar{h}_{i-\frac{1}{2}}(b_i - b_{i-1}) \end{bmatrix} \tag{2.13}$$

where $\bar{h}_{i-\frac{1}{2}} = \frac{1}{2}(h_i + h_{i-1})$. The source term at an interface is therefore fixed during the Riemann problem, and not a function of the solution $\mathbf{q}_l^*$ and $\mathbf{q}_r^*$, to either side.

2.4 A Riemann Solver that Accommodates Source Terms

Considering the treatment of the source term described above, the goal is to approximately solve the following Riemann problem that arises at a cell interface $x = x_{i-\frac{1}{2}}$

$$\mathbf{q}_t + \mathbf{f}'(\mathbf{q})\mathbf{q}_x = \boldsymbol{\Psi}\delta(x - x_{i-\frac{1}{2}})$$
$$\mathbf{q}(x, 0) = \begin{cases} \mathbf{q}_l = \mathbf{Q}_{i-1} & x < x_{i-\frac{1}{2}} \\ \mathbf{q}_r = \mathbf{Q}_i & x > x_{i-\frac{1}{2}} \end{cases}. \tag{2.14}$$

In this section, the features described in the previous section are used to modify the HLLE method in order to adapt the method for the inclusion of a source term. Consider the HLL-type methods described in Section 1.9, where, given predetermined estimates for the wave-speeds arising from the Riemann solution, the original conservation law (1.13) (without a source term) is applied to a region surrounding the Riemann solution in order to determine the middle solution $\mathbf{q}^*$. Inclusion of a source term in the conservation law alters equation (1.30). Furthermore, considering the jump condition at the cell interface, equation (2.12), the solution is no longer constant at the cell interface. If a Riemann solution overlaps the cell interface, the interior of the Riemann solution is no longer a single middle state $\mathbf{q}^*$, but two middle states: $\mathbf{q}_l^*$ to the left, and $\mathbf{q}_r^*$ to the right of the interface; see Figure 2.1. Considering these facts and applying conservation laws with a source term (1.8) to a region $[x_l, x_r]$ surrounding a Riemann solution, gives

$$
\begin{aligned}
\frac{d}{dt} \int_{x_l}^{x_r} \mathbf{q}(x,t)\, dx &= -\left[\mathbf{f}(\mathbf{q}(x_r, t)) - \mathbf{f}(\mathbf{q}(x_l, t))\right] + \int_{x_l}^{x_r} \mathbf{\Psi}\delta(x)\, dx \\
\Rightarrow -s^2 \left(\mathbf{q}_r - \mathbf{q}_r^*\right) - s^1 \left(\mathbf{q}_l^* - \mathbf{q}_l\right) &= -\left[\mathbf{f}(\mathbf{q}_r) - \mathbf{f}(\mathbf{q}_l)\right] + \mathbf{\Psi}
\end{aligned}
\tag{2.15}
$$

where for notational simplicity $\mathbf{q}_{l,r} = \mathbf{q}(x_{l,r}, t)$.

It is not obvious what estimates for s^1 and s^2 in (2.15) are appropriate, given that there is now a source term in the Riemann problem. The same HLLE speeds, (2.3) and (2.4), are proposed as suitable estimates for the wave-speeds since the addition of a source term to a hyperbolic system does not change the eigenvalues of the Jacobian matrix. That is, even for the nonhomogeneous shallow water equations, the characteristic speeds are still $u \pm \sqrt{gh}$. Additionally, it can be shown that the Rankine-Hugoniot condition is unchanged if the source term is finite. Therefore, wave-speeds are the same in analytical solutions to the homogeneous and nonhomogeneous shallow water equations. Of course, over time, the source term has an indirect effect on the speed of wave propagation by its effect on the solution and hence $u \pm \sqrt{gh}$. This indirect effect will be reflected in the numerical solution as well, as the source term affects the solution in each time-step. Therefore, at least heuristically, using the same HLLE speeds for s^1 and s^2 in (2.15) is justified.
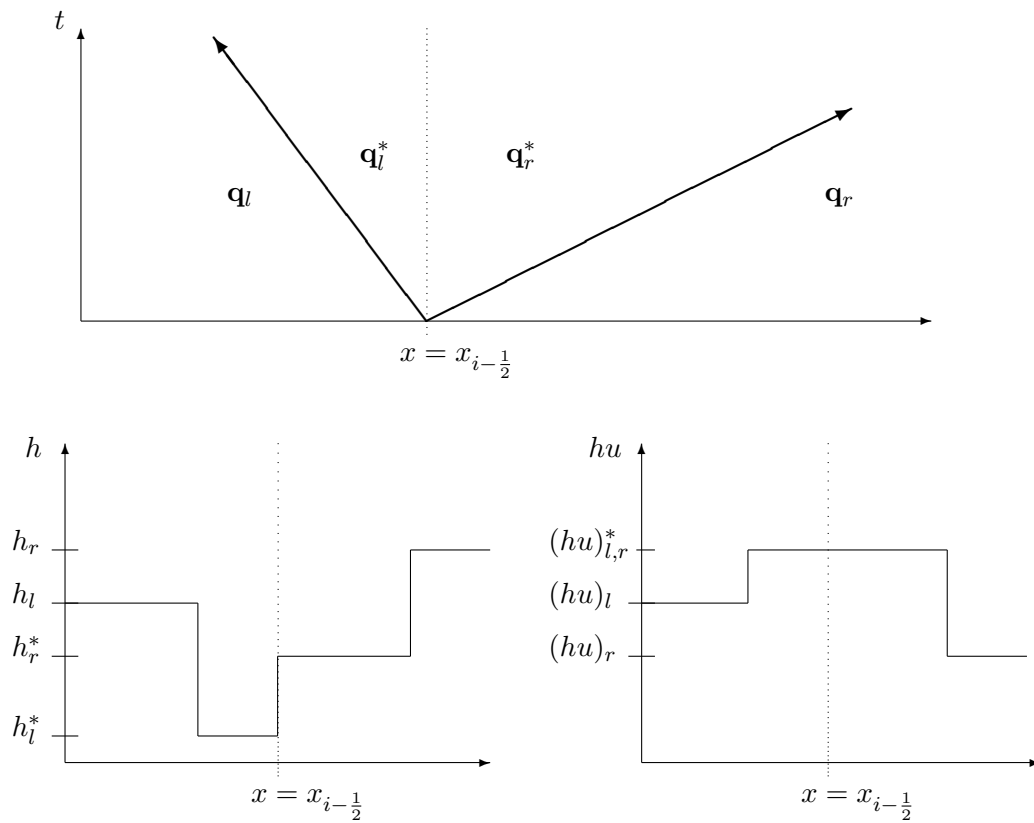
Figure 2.1: Depiction of the approximate Riemann solution of when the HLLE method is extended to accommodate a source term. Top: The discontinuities in the x–t plane, when the approximate Riemann solution overlaps a cell interface. Bottom Left: The water depth h of the approximate Riemann solution at a particular time. Bottom Right: The momentum depth hu of the approximate Riemann solution at a particular time.

For a system of two equations such as the shallow water equations, (2.15) is two equations for the unknown middle states, $\mathbf{q}_l^*$ and $\mathbf{q}_r^*$. The jump condition (2.12)

$$\mathbf{f}(\mathbf{q}_r^*) - \mathbf{f}(\mathbf{q}_l^*) = \boldsymbol{\Psi}, \tag{2.16}$$

provides two more equations for the four unknowns. Together (2.15) and (2.16) is a closed system of four equations for the four unknown variables—both components of the two middle states $\mathbf{q}_l^*$ and $\mathbf{q}_r^*$. However, it is not yet clear if the middle states can be uniquely determined from the system of equations; for the shallow water equations, (2.16) is a nonlinear system. Furthermore, if a unique solution can be found, it is not yet clear if positivity will be ensured for the middle-state depth variables h_l^* and h_r^*. In order to address these questions, it is necessary to investigate the specific properties of (2.15) and (2.16) for the shallow equations.

For the shallow water equations, (2.15) gives the following two equations:

$$-s^2 (h_r - h_r^*) - s^1 (h_l^* - h_l) = -[(hu)_r - (hu)_l] \tag{2.17}$$

$$-s^2 ((hu)_r - (hu)_r^*) - s^1 ((hu)_l^* - (hu)_l) = \tag{2.18}$$
$$- \left[(hu^2 + \frac{1}{2}gh^2)_r - (hu^2 + \frac{1}{2}gh^2)_l \right] - g\bar{h}_{i-\frac{1}{2}} (b_i - b_{i-1})$$

and the jump condition (2.16) gives the equations:

$$(hu)_r^* - (hu)_l^* = 0 \tag{2.19}$$

$$(hu^2 + \frac{1}{2}gh^2)_r^* - (hu^2 + \frac{1}{2}gh^2)_l^* = -g\bar{h}_{i-\frac{1}{2}} (b_i - b_{i-1}). \tag{2.20}$$

Since there is no source of mass at the interface, equation (2.19) implies that the mass flux, which happens to be the second component of the solution—the momentum—is continuous across the interface. Therefore, there is only one middle state for the second component of the solution, $(hu)^* = (hu)_l^* = (hu)_r^*$, and it can be determined immediately from conservation by solving (2.18)

$$-s^2 ((hu)_r - (hu)^*) - s^1 ((hu)^* - (hu)_l) = -[\mathbf{f}(\mathbf{q}(x_r, t)) - \mathbf{f}(\mathbf{q}(x_l, t))] - g\bar{h}_{i-\frac{1}{2}} (b_i - b_{i-1})$$
$$\Rightarrow (hu)^* = \left(\frac{1}{s^2 - s^1} \right) \left((hu^2 + \frac{1}{2}gh^2)_l - (hu^2 + \frac{1}{2}gh^2)_r - s^1 (hu)_l + s^2 (hu)_r \right).$$
$$\tag{2.21}$$

It remains to find the two depths h_l^* and h_r^* in the middle states from conservation and the remaining jump condition. Considering conservation first, the total depth integrated over the approximate Riemann solution will be positive. To see why, consider the source term: the first component is zero as there is no source of mass. Therefore, if the depth arising in the approximate Riemann solution is integrated across the entire Riemann solution, the value will be identical to that of the homogeneous case since they both obey the same conservation equation

$$\frac{d}{dt} \int_{x_l}^{x_r} h(x,t)\,dx = -\left[hu(x_r,t) - hu(x_l,t)\right], \tag{2.22}$$

and the entire middle solution in the homogeneous case is positive as proved in Section 2.2. This suggests a convenient way to solve for the two middle states h_l^* and h_r^*. First, a single middle state is calculated which if integrated would give the amount of mass in the Riemann solution, then, by enforcing conservation of this amount and applying the jump condition (2.20), the single middle state can be divided into two. Now it is possible that enforcing the jump condition could produce one negative middle depth that is offset by the other positive middle depth when integrated across the Riemann solution. However, upon inspecting the jump condition (2.20), and noting that $(hu)^*$ is predetermined, there must always be a solution that satisfies conservation and the jump-condition as either h_l^* or h_r^* approaches zero.[1] The difficulty with the nonlinear jump condition comes not in finding a solution, but in isolating the correct solution; more than one solution corresponding to positive middle states may exist. There are two possible resolutions to this difficulty: one, adding some other criterion to constrain the possible solutions, or two, accepting an approximation to the nonlinear jump condition that can be solved uniquely.

Since the Riemann solver developed in this chapter is an approximate solver, the idea of circumventing the nonlinear jump condition by using an approximation comes naturally.

---

[1]The two middle states h_l^* and h_r^* appearing in the jump condition are related by conservation of a single finite middle state, so if one increases the other must decrease. Since hu^* is a single predetermined constant c, determined by conservation, then $hu^2 = (hu)^2/h = c^2/h \to \infty$ as $h \to 0$. Inserting this into the jump condition gives $(c)^2(1/h_r^* - 1/h_l^*) + (\frac{1}{2}gh_r^{*2} - \frac{1}{2}gh_l^{*2}) = -g\bar{h}_{i-\frac{1}{2}}(b_i - b_{i-1})$. A root can always be found by letting either h_l^* or h_r^* approach zero, depending on the sign of $-g\bar{h}_{i-\frac{1}{2}}(b_i - b_{i-1})$.

Furthermore, an approximation to the jump condition can be based on physical grounds. Equation (2.20) implies that the difference in momentum flux on either side of the delta source must balance the source. Of the two terms in the momentum flux, one comes from advection of momentum and the other comes from a horizontal pressure gradient due to variable depth. In the standard derivation of the shallow water equations it is assumed that $u = O(\sqrt{gh})$, which is consistent with the vertical hydrostatic assumption. However, for flows that are nearly static, the pressure gradient alone must nearly balance source terms from topography. For flows in this regime it can be assumed that $u \ll \sqrt{gh}$, which is consistent with the vertical hydrostatic assumption as well as an additional assumption. Many geophysical flows of interest fall into this regime; see [19]. Imposing this assumption on the jump condition, equation (2.20), leads to the following lowest order asymptotic approximation:

$$(\frac{1}{2}gh^2)_r^* - (\frac{1}{2}gh^2)_l^* = -g\bar{h}_{i-\frac{1}{2}}(b_i - b_{i-1}). \tag{2.23}$$

Equation (2.23) can be loosely interpreted as a statement that variable bottom topography results in variable depth such that the water surface elevation is approximately constant.[2] Although equation (2.23) is nonlinear, when combined with the conservation constraint relating h_l^* and h_r^*, an explicit solution can be found. It is possible that the solution corresponds to one negative middle state and one positive, which is resolved by setting the negative state to zero and choosing the other state such that conservation is maintained. This is not as pathological as it sounds, as it occurs when the pressure gradient cannot completely balance the source term, or when a body of water is adjacent to a dry region with steep sloping topography. In such a case the discrete version of the source term may not be physically realistic anyway, as it involves the height of the topography in the dry region which is irrelevant.

For flows that are far from static the above approximation may be inappropriate. However, it suggests a way to find the physically relevant solution to the nonlinear jump

---

[2]In fact, an alternative formulation of the source term using $\bar{h} = \frac{1}{2}(h_l^* + h_r^*)$, reduces equation (2.23) to $h_r^* + b_r = h_l^* + b_l$.

condition—equation (2.20). If the term hu^* in equation (2.20) increases continuously from zero, the physically relevant solution should vary continuously from the approximate solution to (2.23).

It should be noted that in the above derivations it was assumed that the Riemann solution overlaps the cell interface. In the event of both positive or both negative speeds s^1 and s^2, the Riemann solution is entirely to one side of the interface. In such an event it is only necessary to calculate a single middle state based on conservation. It can be shown that enforcing the jump condition at the cell interface in such a situation has no effect on the solution, and therefore the Riemann problem is simplified considerably in this case since $\mathbf{q}_r^* = \mathbf{q}_l^*$.

2.5 *Improving Dry Interfaces with Altered Speed Estimates*

The resolution of moving wet-dry interfaces can be improved by using alternative estimates for the speeds s^1 and s^2 in such a case. The idea is to use knowledge of the exact Riemann solution when the left or right state has zero depth. Such solutions have a single rarefaction (and a zero-strength shock) in either the first or second characteristic family, depending on which side is dry; see figure (2.2). Therefore, the true maximum speeds arising from the Riemann problem correspond to the right and left edges of the rarefaction fan, and these known speeds can be used as s^1 and s^2 in determining the middle-states $\mathbf{q}_l^*$ and $\mathbf{q}_r^*$. For a complete description of the exact Riemann solution in such a case see [18].

2.6 *A Positive-Depth Preserving Godunov-Type Scheme*

The numerical method is implemented as a wave-propagation algorithm as described in [15]. That is, once the approximate Riemann solution at each cell interface is constructed as described in the previous discussion, with $\mathbf{q}_r = \mathbf{Q}_i$ and $\mathbf{q}_l = \mathbf{Q}_{i-1}$, the wave structure of each Riemann solution is used to update the solution, by re-averaging the grid cells due to the waves. Although an interface flux isn't specifically used as suggested in (1.14),
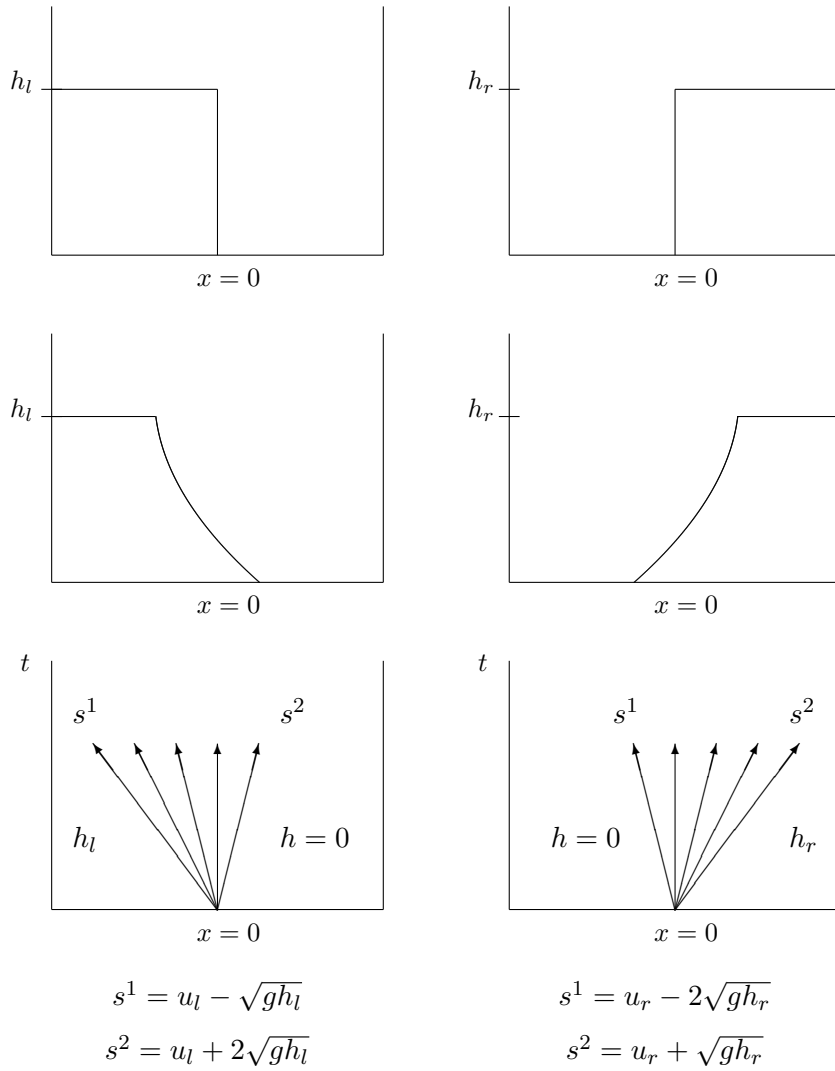
Figure 2.2: Exact Riemann Solution when the right or left state is dry. Top: Initial depth of water is dry on the left or right. Middle: The water depth at some time after the initial profile. Bottom: Riemann solution in the x–t plane. The dry state is connected to the wet one through a single rarefaction. The speeds of the far edges of the rarefaction are shown.

the method is still conservative since the approximate Riemann solution was based on applying conservation to the region surrounding the Riemann solution. Before writing a general updating formula, it is convenient to introduce some notation for the Riemann solution at the interface between the cells i and $i - 1$. Following Section (1.6) for linear problems, the following notation will be used for the discontinuities or waves arising from the Riemann problems: $\mathcal{W}^1_{i-\frac{1}{2}} = \mathbf{q}^*_l - \mathbf{Q}^n_{i-1}$ and $\mathcal{W}^2_{i-\frac{1}{2}} = \mathbf{Q}^n_i - \mathbf{q}^*_r$. For the speeds of these propagating waves, the following notation will be used: $(s^p_{i-\frac{1}{2}})^- = \min(0, s^p_{i-\frac{1}{2}})$ and $(s^p_{i-\frac{1}{2}})^+ = \max(0, s^p_{i-\frac{1}{2}})$. Using this notation, the updating formula can be written as

$$\mathbf{Q}^{n+1}_i = \mathbf{Q}^n_i - \frac{\Delta t}{\Delta x} \sum_{p=1}^n \left[(s^p_{i+\frac{1}{2}})^- \mathcal{W}^p_{i+\frac{1}{2}} + (s^p_{i-\frac{1}{2}})^+ \mathcal{W}^p_{i-\frac{1}{2}} \right]. \tag{2.24}$$

Stability restrictions for Godunov-type methods typically require $\max_i(s^1_{i-\frac{1}{2}}, s^2_{i-\frac{1}{2}})\Delta t < \Delta x$; see [15]. This implies that a particular wave arising from a Riemann problem remains entirely within a grid cell of width Δx. Increasing this restriction on the time step to $\max_i(s^1_{i-\frac{1}{2}}, s^2_{i-\frac{1}{2}})\Delta t < \frac{1}{2}\Delta x$ guarantees maintaining a non-negative numerical solution given non-negative Riemann solutions $\mathbf{q}^*_{l,r}$. This can be understood by interpreting the updating as re-averaging the solution due to a set of piecewise-constant discontinuities that move into a grid cell from either side, stopping short of the middle of the cell. The smallest possible value behind any discontinuity is zero, and so the new average value in a cell can be no less than zero.

2.7 *Extension to a Second-Order Accurate Method*

The Godunov-type methods discussed so far are limited to first-order accuracy, since they are based on a piecewise constant reconstruction of the solution at each time-step. However, this restriction can be lifted to second-order accuracy based on a higher-order approximation to the PDEs.

The analysis of the numerical error is facilitated considerably by first applying the methods to a linear conservation law. Recall that in Section (1.6) it was shown that such laws

can be reduced to a set of decoupled scalar advection equations of the form

$$w_t^p + \lambda^p w_x^p = 0 \tag{2.25}$$

for each characteristic family $p = 1 \ldots n$. Consider a Taylor expansion of the solution to (2.25) with respect to time

$$w^p(x, t + \Delta t) = w^p(x, t) + \Delta t w_t^p(x, t) + \frac{\Delta t^2}{2} w_{tt}^p(x, t) + O(\Delta t^3). \tag{2.26}$$

By using (2.25), the time derivatives in (2.26) can be replaced with spatial derivatives, giving

$$w^p(x, t + \Delta t) = w^p(x, t) - \lambda^p \Delta t w_x^p(x, t) + \frac{(\lambda^p \Delta t)^2}{2} w_{xx}^p(x, t) + O(\Delta t^3). \tag{2.27}$$

The Godunov methods discussed so far, if applied to a linear conservation law, are equivalent to a first-order upwind finite difference approximation[3] to (2.25) for each family, based on the first two terms on the right hand side of (2.27). The methods are upwind since using the Riemann solution as described is equivalent to using a one-sided approximation to $w_x^p(x, t)$ that correctly takes into account the direction of wave propagation—the sign of λ^p—for the pth family. For a first-order method, an upwind approximation to $w_x^p(x, t)$ is required for stability. If the method is to be second-order, at least in smooth regions, it is necessary to include approximations for the next term in the Taylor expansion (2.27). The approximate Riemann solution is still of interest since it can be used to construct the approximation to $\frac{(\lambda^p \Delta t)^2}{2} w_{xx}^p(x, t)$, as well as for other reasons discussed in the next section.

If a Godunov method is written as a flux-differencing method (1.14) and applied to a single characteristic family, or scalar conservation law (2.25), the flux is equivalent to

$$F_{i-\frac{1}{2}}^p = (\lambda^p)^- w_i^p + (\lambda^p)^+ w_{i-1}^p. \tag{2.28}$$

A correction term can be added to (2.28), which when used in (1.14), gives a second-order centered approximation to $\frac{(\lambda^p \Delta t)^2}{2} w_{xx}^p(x, t)$. It is easy to show that the appropriate

---

[3]This is if the variable $\mathbf{Q}_i$ in a finite-volume method is regarded as the value at the cell center, rather than the average value throughout the cell, a difference of $O(\Delta x^2)$ for smooth solutions.

correction term is:

$$-\frac{\Delta t}{2\Delta x}(\lambda^p)^2 \left(w_i^p - w_{i-1}^p\right). \tag{2.29}$$

Furthermore, the first-order upwind approximation to $w_x^p(x,t)$ can be extended to a second-order centered approximation by including another term in the flux (2.28)

$$\frac{1}{2}|\lambda^p|\left(w_i^p - w_{i-1}^p\right). \tag{2.30}$$

A centered approximation to $w_x^p(x,t)$ is stable as long as (2.29) is included as well. These two correction terms to the first-order flux can be thought of as a correction flux $\tilde{F}_{i-\frac{1}{2}}^p$ that modifies the first-order upwind method to a second-order centered method. The flux (2.28) to be used in (1.14) then becomes

$$F_{i-\frac{1}{2}}^p = (\lambda^p)^- w_i^p + (\lambda^p)^+ w_{i-1}^p + \tilde{F}_{i-\frac{1}{2}}^p \tag{2.31}$$

where

$$\tilde{F}_{i-\frac{1}{2}}^p = \frac{1}{2}\left(|\lambda^p| - \frac{\Delta t}{2\Delta x}(\lambda^p)^2\right)\left(w_i^p - w_{i-1}^p\right). \tag{2.32}$$

Using the flux (2.31) in (1.14) with (2.32) as the correction flux is equivalent to the well known Lax-Wendroff method for scalar advection. See for example [15].

Upon considering the solution to a linear system from Section (1.6), it is clear that if the above correction terms are extended to a linear system, the correction flux becomes

$$\tilde{\mathbf{F}}_{i-\frac{1}{2}} = \sum_{p=1}^{n}\left[\frac{1}{2}\left(|\lambda^p| - \frac{\Delta t}{2\Delta x}(\lambda^p)^2\right)\mathcal{W}_{i-\frac{1}{2}}^p\right] \tag{2.33}$$

where $\mathcal{W}_{i-\frac{1}{2}}^p$ is the pth discontinuity $\left(w_i^p - w_{i-1}^p\right)\mathbf{r}^p$ discussed in Section (1.6). If the system is nonlinear, the flux correction term (2.33) for a linear system can be used, but with the approximate Riemann solution at each interface determining the speeds and waves, rather than the exact linear solution

$$\tilde{\mathbf{F}}_{i-\frac{1}{2}} = \sum_{p=1}^{n}\left[\frac{1}{2}\left(|s_{i-\frac{1}{2}}^p| - \frac{\Delta t}{2\Delta x}(s_{i-\frac{1}{2}}^p)^2\right)\mathcal{W}_{i-\frac{1}{2}}^p\right]. \tag{2.34}$$

Using the first-order Godunov method (2.24) from the previous section together with the correction fluxes, (2.34), gives the second-order updating formula

$$\mathbf{Q}_i^{n+1} = \mathbf{Q}_i^n - \frac{\Delta t}{\Delta x} \sum_{p=1}^{n} \left[(s_{i+\frac{1}{2}}^p)^- \mathcal{W}_{i+\frac{1}{2}}^p + (s_{i-\frac{1}{2}}^p)^+ \mathcal{W}_{i-\frac{1}{2}}^p \right] - \frac{\Delta t}{\Delta x} \left[\tilde{\mathbf{F}}_{i+\frac{1}{2}} - \tilde{\mathbf{F}}_{i-\frac{1}{2}} \right]. \qquad (2.35)$$

2.8   Flux-Limiters and High-Resolution Methods

In the previous section it was shown how the upwind first-order Godunov method can be converted to a centered second-order method. The question may arise, if a centered method with no upwind bias is used, what point is there in solving or approximating a Riemann problem? The answer is that, in smooth regions, a Riemann problem might be avoided altogether, however, hyperbolic conservation laws such as the shallow water equations admit discontinuous solutions, and the analysis of the previous section assumed smoothness of the solution. For regions with a discontinuity, not only does the updating formula (2.35) of the previous section fail to be second-order accurate, it can lead to large spurious oscillations near the discontinuity, and cannot accurately capture a moving discontinuity's speed. In such regions, the first-order Godunov method of Section (2.4) is superior, as it can converge to a correct weak solution and can accurately capture a moving discontinuity's speed; see [17] or [15]. Ideally then, one would like to use the second-order accurate centered method (2.35) where the solution is smooth, and use a Godunov method (2.24) where the solution contains a discontinuity. This is the idea behind the "high-resolution" methods, where an attempt is made to identify areas where a discontinuity exists, and then resort to the Godunov method in the region surrounding the discontinuity. This can be done by modifying the updating formula presented in the previous section,

$$\mathbf{Q}_i^{n+1} = \mathbf{Q}_i^n - \frac{\Delta t}{\Delta x} \sum_{p=1}^{n} \left[(s_{i+\frac{1}{2}}^p)^- \mathcal{W}_{i+\frac{1}{2}}^p + (s_{i-\frac{1}{2}}^p)^+ \mathcal{W}_{i-\frac{1}{2}}^p \right] - \frac{\Delta t}{\Delta x} \left[\tilde{\mathbf{F}}_{i+\frac{1}{2}} - \tilde{\mathbf{F}}_{i-\frac{1}{2}} \right] \qquad (2.36)$$

by adding a coefficient to the correction fluxes

$$\tilde{\mathbf{F}}_{i-\frac{1}{2}} = \phi_{i-\frac{1}{2}} \sum_{p=1}^{n} \left[\frac{1}{2} \left(|s_{i-\frac{1}{2}}^p| - \frac{\Delta t}{2\Delta x} (s_{i-\frac{1}{2}}^p)^2 \right) \mathcal{W}_{i-\frac{1}{2}}^p \right]. \qquad (2.37)$$

The coefficient $\phi_{i-\frac{1}{2}}$ is known as a "flux-limiter" and can take values between 0 and 1. If $\phi_{i\pm\frac{1}{2}} = 1$, equation (2.36) is equivalent to the method of the previous section, equation (2.35), and if $\phi_{i\pm\frac{1}{2}} = 0$, it is equivalent to the first-order Godunov method, equation (2.24). A low value of the limiters $\phi_{i\pm\frac{1}{2}}$ is intended to reflect a discontinuity, or a rapidly changing gradient in the solution near the ith grid cell. The latter case can cause spurious oscillations in the numerical solution, even if the solution is smooth; see [15].

Many formulas for limiters have been used with these goals in mind. In practice, it usually makes more sense to limit the correction flux by limiting the contribution from each wave $\mathcal{W}^p_{i-\frac{1}{2}}$ separately. The rationale is that the solution is composed of the superposition of more than one characteristic family, so a discontinuity in the solution is likely a discontinuity in one characteristic value, while the others may be smooth in the same region. Therefore, often limiters are applied separately to each wave based on estimating the gradient of the corresponding characteristic value, in which case (2.37) becomes

$$\tilde{\mathbf{F}}_{i-\frac{1}{2}} = \sum_{p=1}^{n} \left[\frac{1}{2} \left(|s^p_{i-\frac{1}{2}}| - \frac{\Delta t}{2\Delta x} (s^p_{i-\frac{1}{2}})^2 \right) \phi^p_{i-\frac{1}{2}} \mathcal{W}^p_{i-\frac{1}{2}} \right] \tag{2.38}$$

with $\phi^p_{i-\frac{1}{2}} \in [0,1]$. For a complete discussion of different limiters, and how the value of the limiter is determined from the numerical solution near a grid cell, see [15].

Aside from the usual motivation for limiters, a new issue arises with very shallow flows with dry regions. As was shown in Section (2.6), the first-order Godunov method presented preserves positivity. However, after adding the flux correction terms in (2.38), it is certainly not evident that positivity will be maintained, as the net effect of the flux correction terms $\tilde{\mathbf{F}}_{i\pm\frac{1}{2}}$ in (2.35) might decrease the solution in the ith grid cell. This poses a new problem, yet one that can be circumvented by a new use for limiters. Since limiters can reduce the method (2.38) to a first-order Godunov method in the presence of discontinuities or steep gradients, they can also be used to reduce the method to a first-order Godunov method when a negative solution in a grid cell arises. The most obvious way to accomplish this is to merely set the limiters to 0, whenever second-order correction fluxes drive a cell value into negative depth. Computationally this is slightly more involved than it sounds, as a

correction flux $\tilde{\mathbf{F}}_{i-\frac{1}{2}}$ affects the ith and $(i-1)^{\text{th}}$ grid cells, and necessarily increases the depth in one by decreasing the other. If a region has very shallow water, eliminating the correction flux at an interface might preclude a negative state in one cell, but induce a negative state in the adjacent cell, due to a correction flux applied at the other interface. Therefore, an iterative procedure where correction fluxes are limited to zero such that adjacent cells are not driven negative must be taken.

A more direct approach is to re-limit the already limited correction fluxes so that they cannot drive the depth in a cell negative. This can be done by limiting the gross correction mass-flux out of a cell to the amount of mass in the cell after the first-order Godunov update. Writing the second-order method (2.36) as the sum of the Godunov update $\mathbf{Q}_i^G$ and the limited correction fluxes gives

$$\mathbf{Q}_i^{n+1} = \mathbf{Q}_i^G - \frac{\Delta t}{\Delta x}\left[\tilde{\mathbf{F}}_{i+\frac{1}{2}} - \tilde{\mathbf{F}}_{i-\frac{1}{2}}\right]. \tag{2.39}$$

The gross outward mass-flux due to these correction fluxes is

$$G_i = \left[\max(0, \tilde{F}_{i+\frac{1}{2}}^1) - \min(0, \tilde{F}_{i-\frac{1}{2}}^1)\right]. \tag{2.40}$$

If $\Delta t G_i$ is larger than the mass after the Godunov update $\Delta x (Q_i^G)^1$, the correction fluxes could potentially create a negative depth. This is precluded by re-limiting the correction fluxes based on which cell they take mass away from

$$\tilde{\mathbf{F}}_{i-\frac{1}{2}} \rightarrow \varphi_{i-\frac{1}{2}}\tilde{\mathbf{F}}_{i-\frac{1}{2}} \tag{2.41}$$

where

$$\varphi_{i-\frac{1}{2}} = \begin{cases} \min(1, \Delta x (Q_i^G)^1 / \Delta t G_i) & \text{if} \quad \tilde{F}_{i-\frac{1}{2}}^1 < 0 \\ \min(1, \Delta x (Q_{i-1}^G)^1 / \Delta t G_{i-1}) & \text{if} \quad \tilde{F}_{i-\frac{1}{2}}^1 > 0 \end{cases}. \tag{2.42}$$

This way the need for an iterative procedure is avoided, and a further advantage is that the correction fluxes are not completely eliminated should they drive the depth in a cell negative, but rather are merely re-limited. It is possible that in some cases the correction fluxes will be unnecessarily re-limited, such as when the net corrective mass-flux is much less than the gross corrective mass-flux. However, this seems to be rare in the cases investigated.

2.9   Conclusions and Future Directions

The Godunov-type method presented here has given some promising results for the one-dimensional nonlinear shallow water equations. Like other Godunov-type methods, it can successfully deal with difficulties such as discontinuities arising in hyperbolic PDEs such as the shallow water equations. Additionally, it maintains positivity of the solution when confronted with very shallow flows and captures moving wet-dry fronts in the domain, even over topography. By incorporating the source term directly into the Riemann solution, it also preserves steady-states, and resolves small perturbations from steady-states. Because of these properties, it is believed to be well suited for many realistic applications that present these difficulties. Ultimately, it might be the basis for a full two-dimensional method. Two-dimensional Godunov methods must deal with additional complications such as cross-derivatives that must be handled with transverse Riemann waves; see [15]. Proper extension of this method must still preserve positivity, while preserving steady-states in two dimensions.

The following chapter contains some numerical results for several problems. The method presented in this paper is implemented using the CLAWPACK software package [13].

Chapter 3

RESULTS

3.1 Comparison With an Exact Analytical Solution

The nonlinear shallow water equations with topography cannot in general be solved exactly. Therefore it is not possible to validate a numerical method in all cases, and the problems where an exact solution is known are important test cases. In 1957 Carrier and Greenspan [3] derived a solution to the shallow water equations where a wave climbs a sloping beach. The solution is an important test case in that, not only is there variable topography, there is a moving wet-dry front in the domain.

The specific problem consists of a linear sloping beach rising above the sea level, and a water level that is initially depressed at the coastline. The fluid is held motionless and then released so that the water rises up the beach. The top of figure 3.1 shows the initial profile. A parameter ϵ is used in the problem, which correlates with the steepness of the initial water surface; to guarantee that the wave doesn't break, ϵ must be less than 0.23. The exact solution is then determined as a function of transformed variables σ, λ, for which $\sigma(x, t)$ and $\lambda(x, t)$ are only implicitly defined, so that finding the exact solution as a function of x and t requires a root finding routine. For a complete description of the solution technique see [3].

Using an exact initial profile, with $\epsilon = 0.2$, the solution was computed numerically and compared to the exact solution at various times. The solution is analyzed at early enough times so that off-shore boundary effects have not had time to corrupt the solution near the beach. Figure 3.1 shows the exact and computed solution after the water has progressed up the beach. The region close to the beach is of most interest and has been enlarged in figure 3.2, with several intermediate times shown. As can be seen in the enlarged figures,
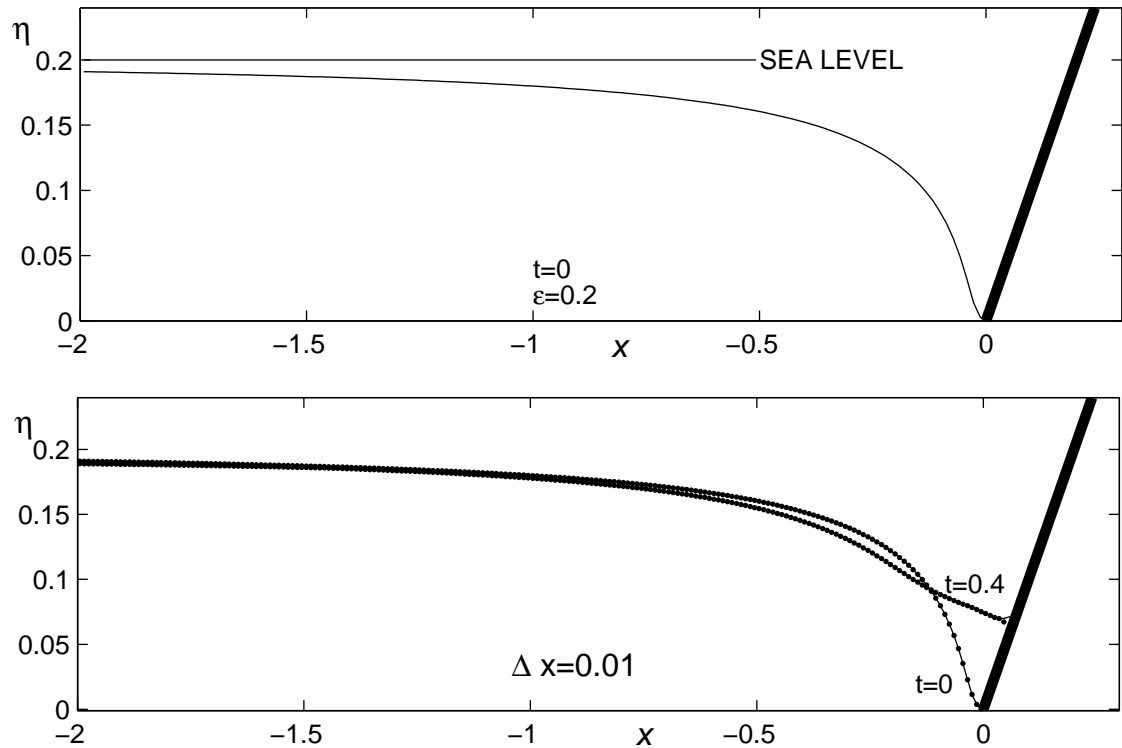
Figure 3.1: Solution from Carrier and Greenspan [3] on the entire computing domain. Top: depiction of the domain and initial profile of the water surface $\eta = h + b$. The heavy line is the sloping beach, and the lighter line the water surface. Bottom: Depiction of the exact and computed solution after the wave has progressed up the beach. The initial profile is shown as well. Exact solution is the solid line, and computed solution is the dotted line, with a dot at each grid cell.

there is clearly the most error near the shoreline and as one might expect the error grows as time proceeds. The solution is shown with and without the use of the alternate speeds from section 2.5, at the wet-dry interface. Even at this coarse resolution, some improvement from using the alternate speeds can be seen.

As the grid is refined, the computational solution approaches the exact solution with the shoreline posing the most difficulty. Figure 3.3 shows the solution as the grid is refined, when the alternate speeds at the wet-dry interface are not used. Although the solution does converge even at the shoreline, at the finest resolution shown error is still visible at the shore, especially at later times. Figure 3.4 shows convergence of the solution as the
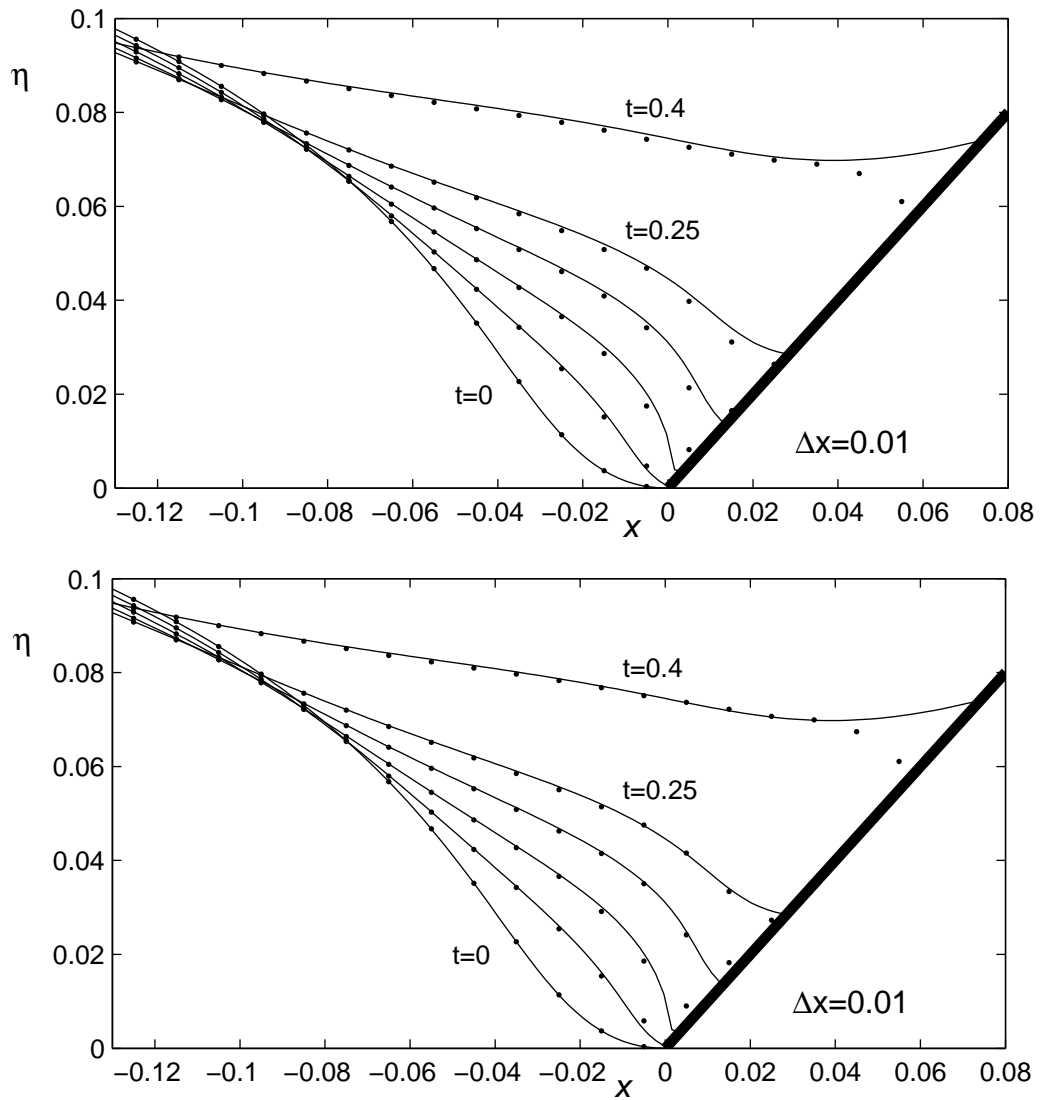
Figure 3.2: A closer view of the exact and computed solutions near the shoreline. At this resolution, the error near the shore can clearly be seen. Top: solution without the use of the alternate speeds at the wet-dry interface. Bottom: solution when the alternate speeds from section 2.5 are used at the wet-dry interface.
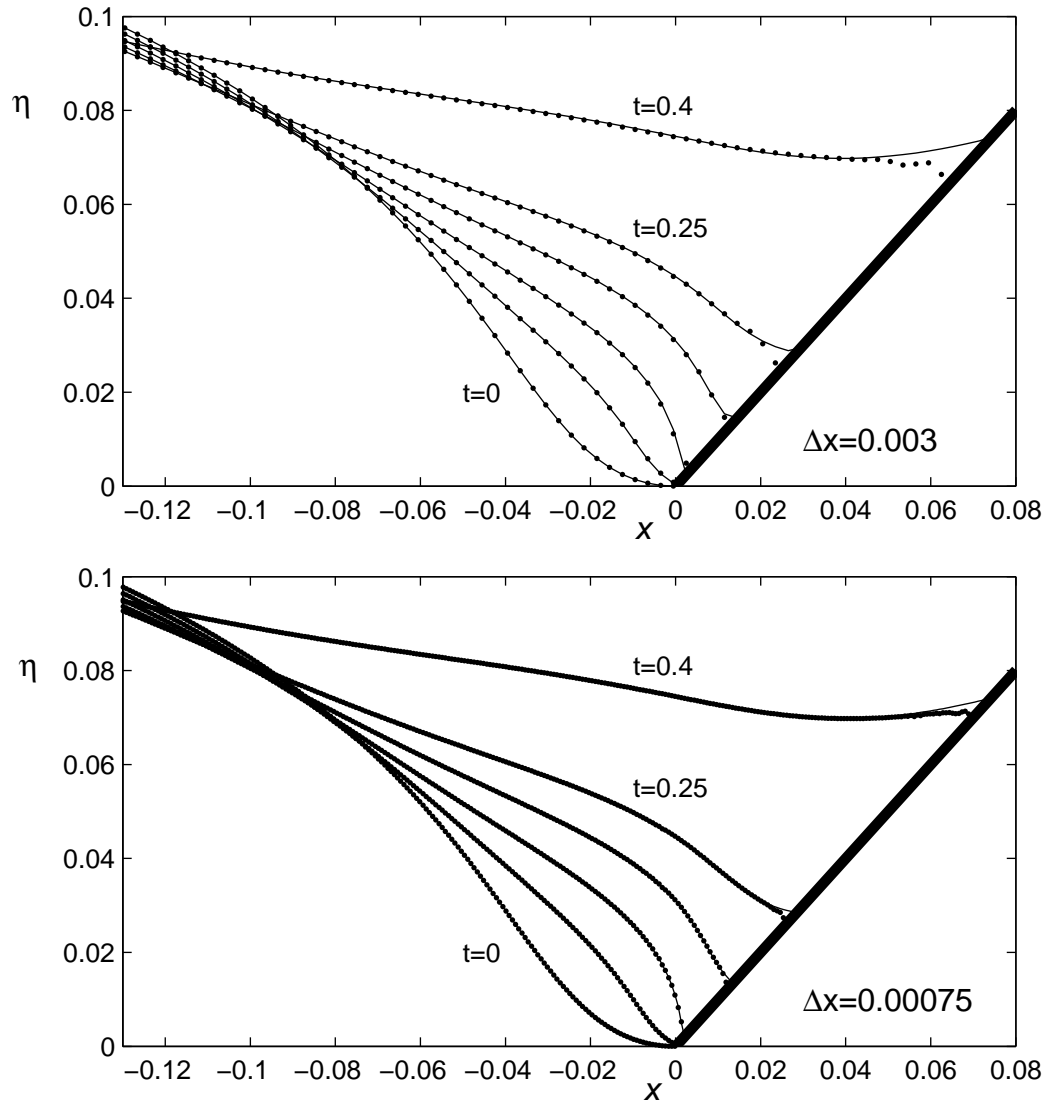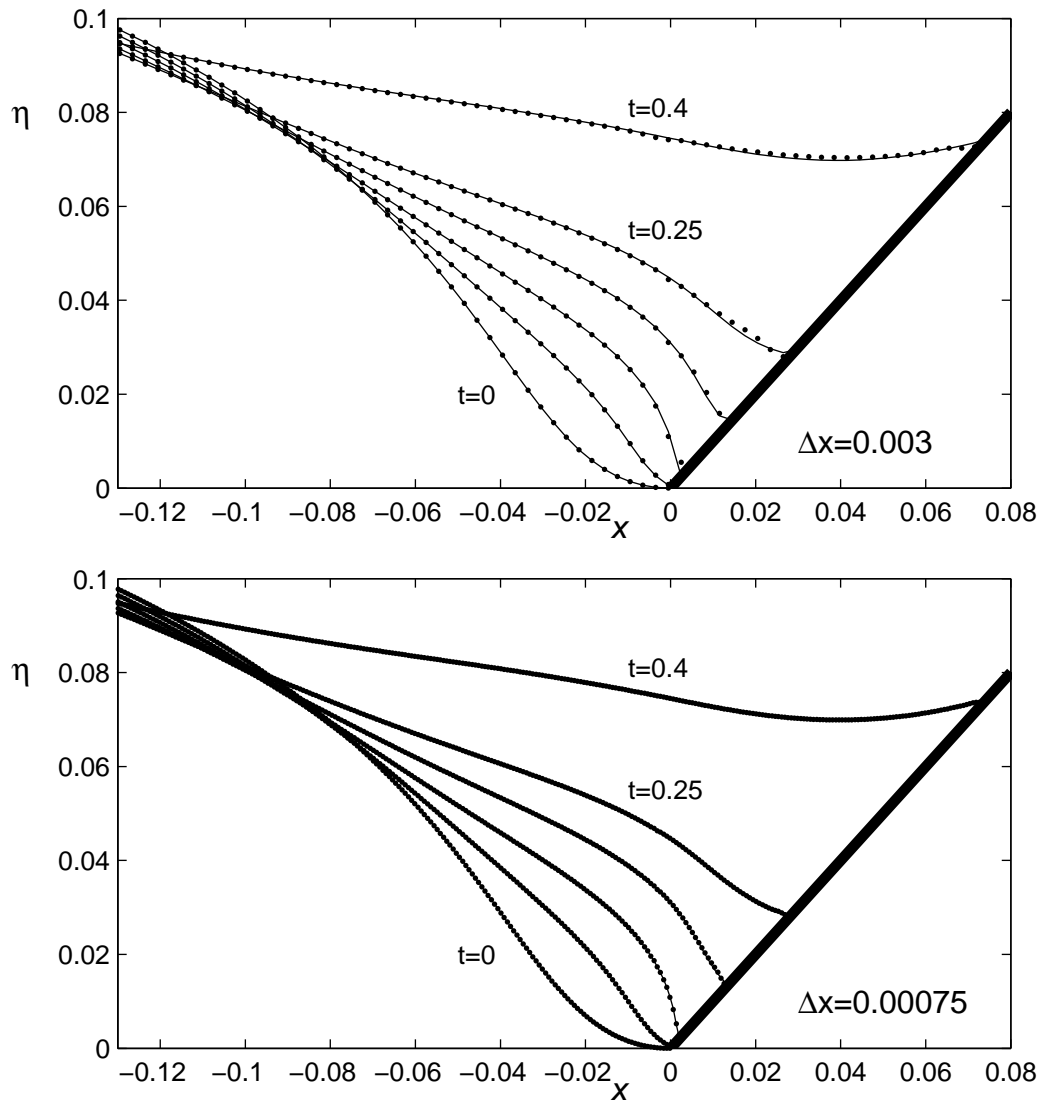
Figure 3.3: Convergence to the exact solution as the grid is refined without the alternate speeds at the wet-dry interface. Exact solutions are the solid lines, and computed solutions are the dotted lines, with a dot at each grid cell. The shoreline clearly poses the most difficulty

Figure 3.4: Convergence to the exact solution as the grid is refined with the alternate speeds at the wet-dry interface. Exact solutions are the solid lines, and computed solutions are the dotted lines, with a dot at each grid cell. Use of the alternate speeds clearly improves the difficulty at the shoreline.
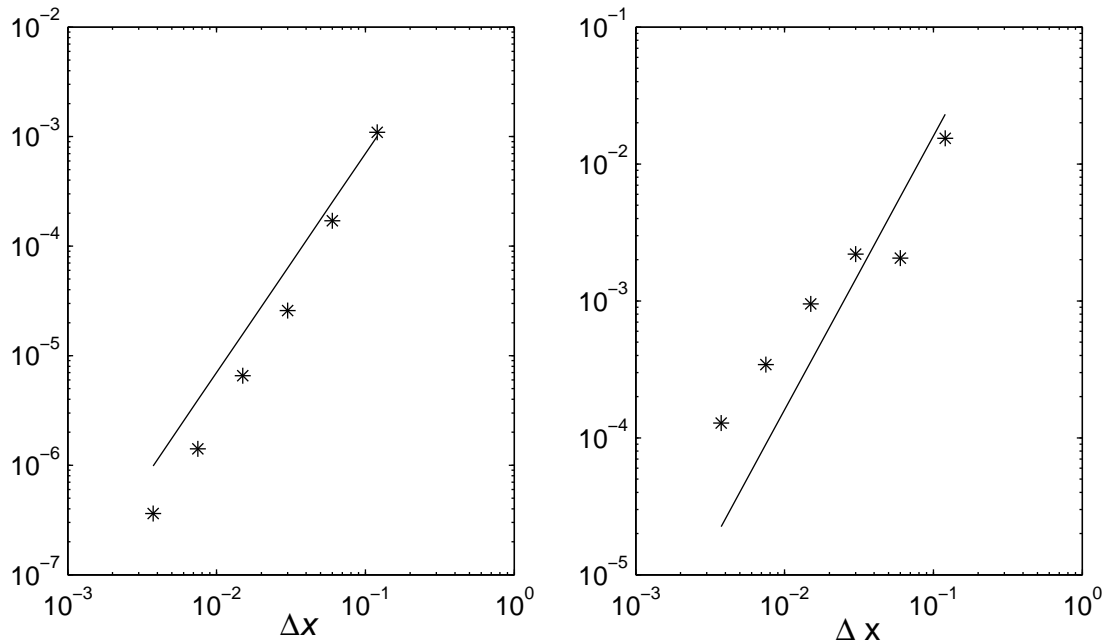
Figure 3.5: Convergence and accuracy of the numerical method. The solid line is $\propto \Delta x^2$, and points * are the error, $(1/2N)\sum_{p=1}^{2}\sum_{i=1}^{N}|q^p(x_i) - Q_i^p|$, given increasing computational resolution. $t = 0.25$. Left: Convergence of the solution away from the shoreline ($-1.0 \leq x \leq 0$). The error is $O(\Delta x^2)$ as $\Delta x \to 0$. Right: Convergence of the solution at the shoreline ($-0.1 \leq x \leq 0.1$). The error is clearly larger at the shoreline, however, convergence is observed.

grid is refined, using the alternate speeds at the wet-dry interface. Although the shoreline still poses the most difficulty, use of the alternate speeds clearly improves the solution at the shoreline. The method converges to the exact solution at the shoreline with nearly second-order accuracy as can be seen in Figure 3.5.

Demonstrating convergence to this exact solution is an important test for the numerical method, since it tests the ability to compute a moving wet-dry interface over sloping topography. Furthermore, as the wave progresses up the beach the method must prevent the appearance of negative states near the shoreline. It should be emphasized that with this numerical method the dry region itself is part of the computational domain, and there is no need for intervention such as tracking the shoreline in order to preserve the non-negative

solution at the shoreline. By keeping the parameter, ϵ, small, the wave is not allowed to break, and this particular solution remains smooth. Therefore, one real strength of a Godunov method is not really tested on this problem as it does not present the difficulties associated with discontinuities and shocks.

3.2   A Test Case

In order to test the robustness of this numerical method, solutions to problems with a wide variety of topographies and initial conditions have been computed. One such problem is shown below, which contains many of the difficulties posed by applications simultaneously. The domain includes moving wet and dry regions over topography, and a stationary steady-state over steep topography. Additionally the problem has several shocks including a stationary bore. The computational solution is shown in the following twenty snapshots in time, Figure 3.6. The problem begins with an initial discontinuity that is released, giving rise to a moving shock wave. Note the preservation of the stationary pool on the right until it is upset with inflowing water. The far right side of the pool is over a steep slope, meaning that a large source term must exactly balance a large flux-gradient in order to preserve the stationary surface. This is followed by a stationary shock as well as a travelling shock that moves to the far right shore and is then reflected.
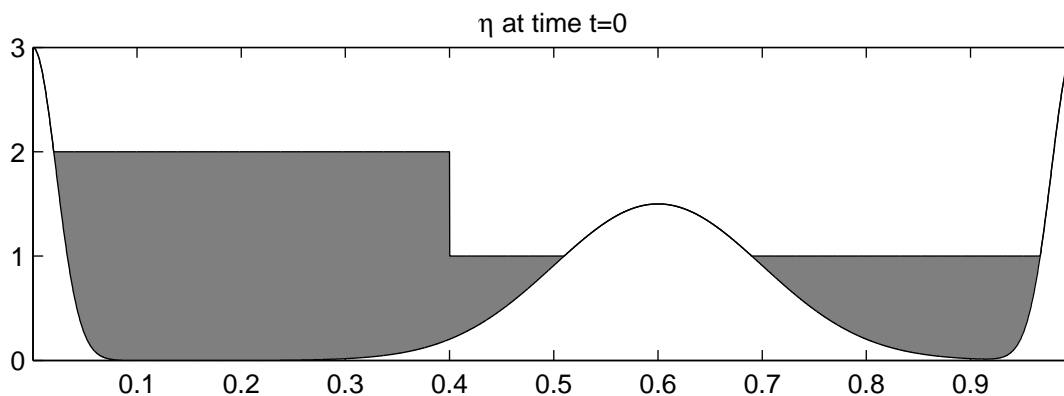

Figure 3.6: Computational solution of a challenging test case. Figures are snapshots in time.

Figure 3.6 continued

η at time t=0.25

η at time t=0.3
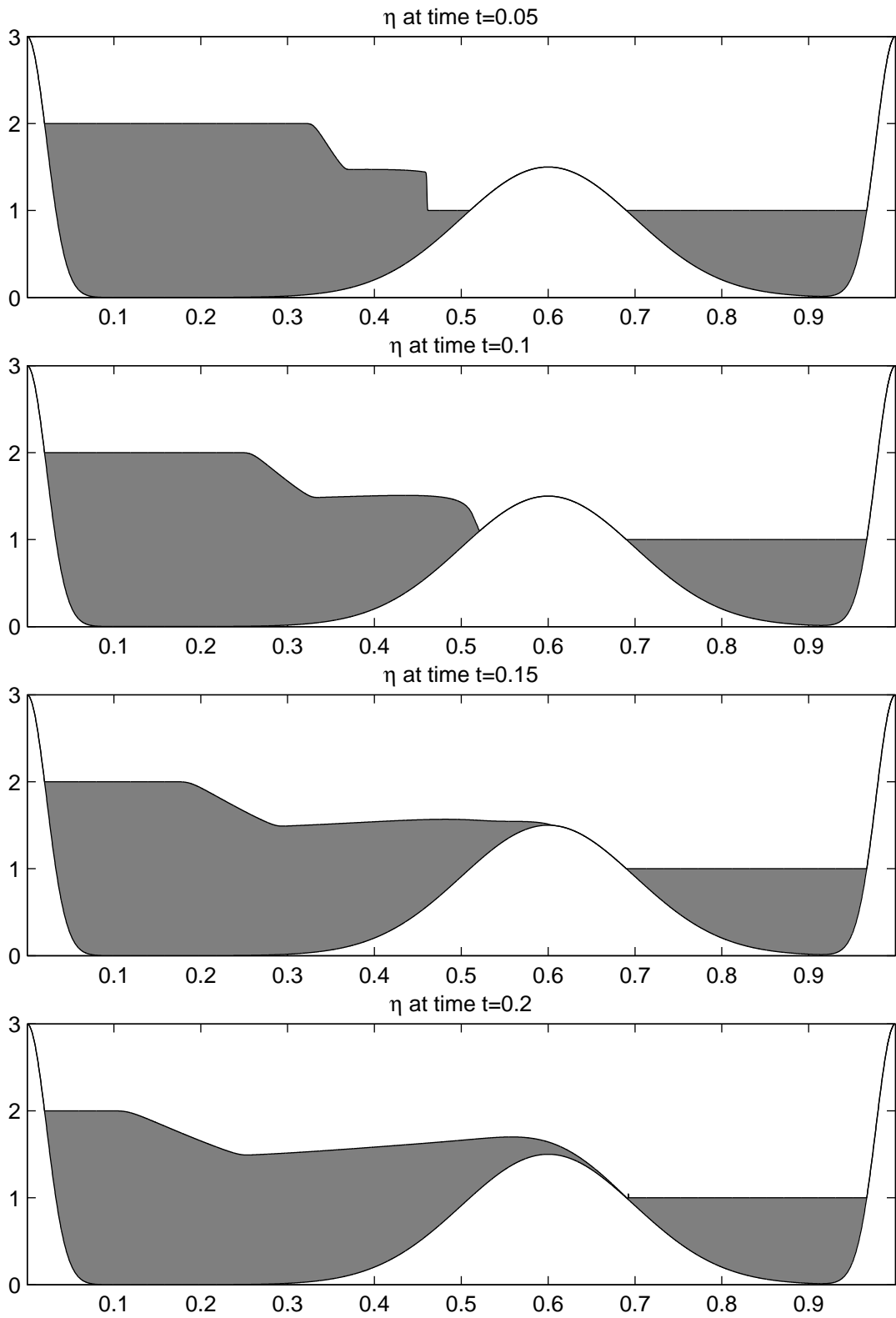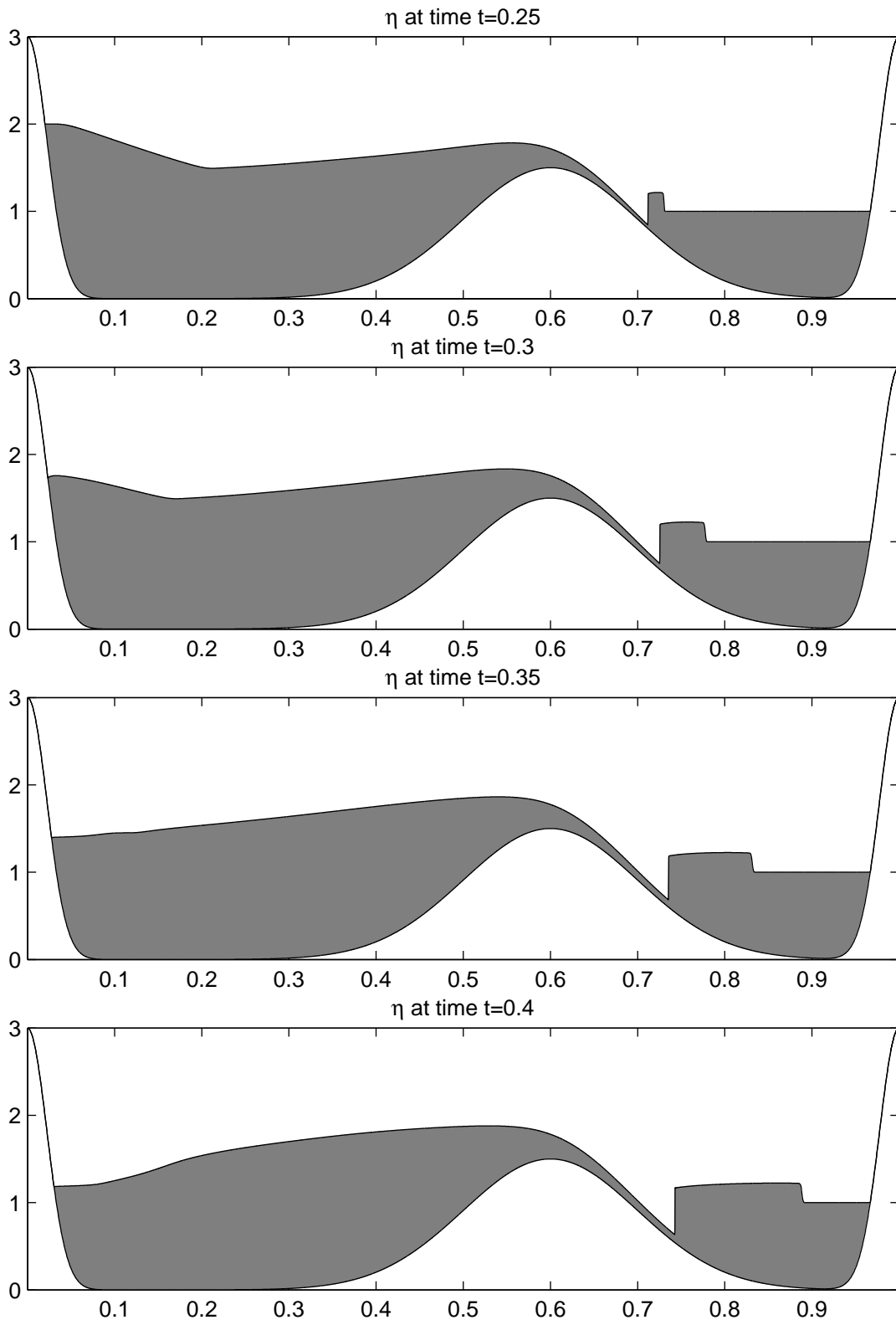
η at time t=0.35

η at time t=0.4
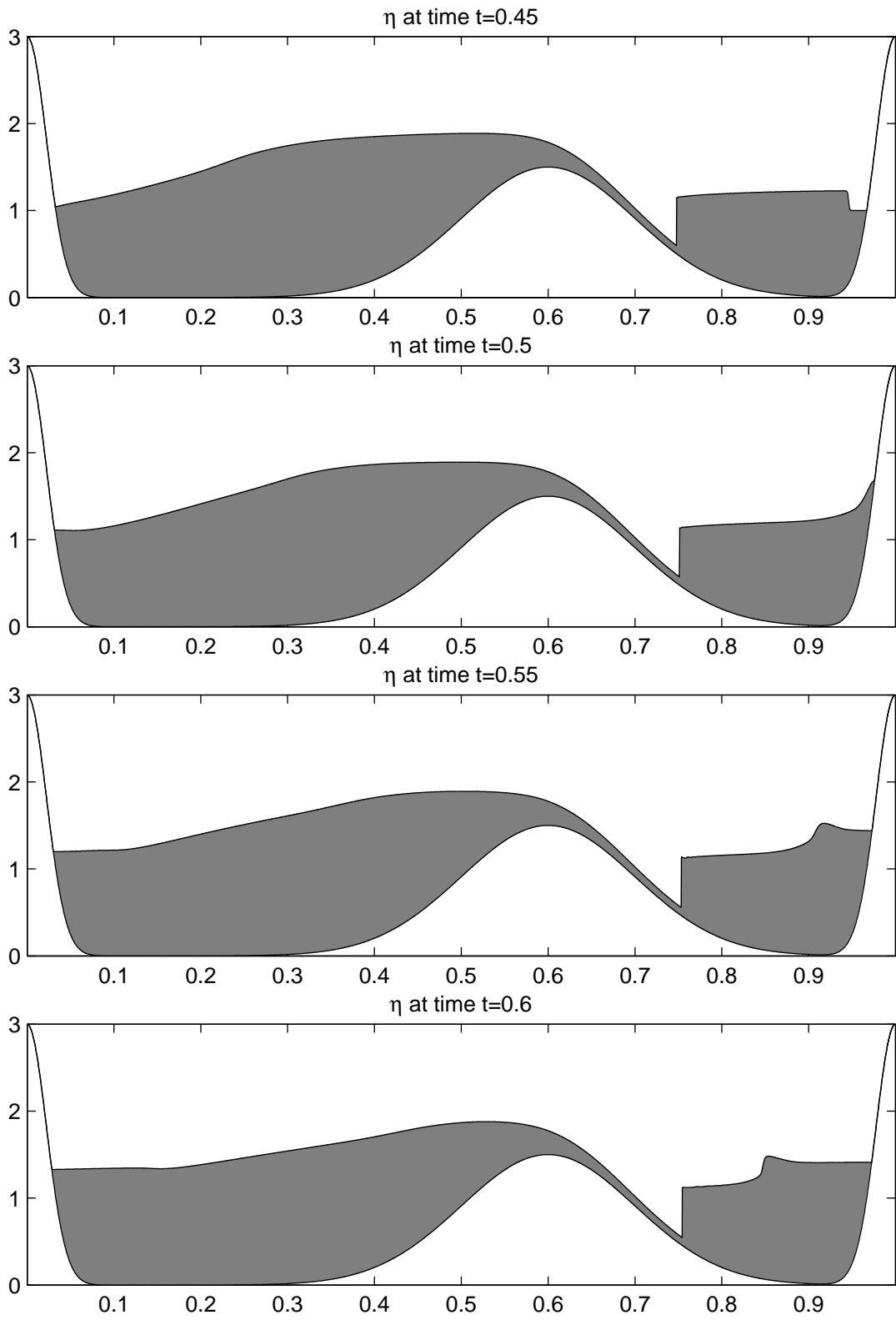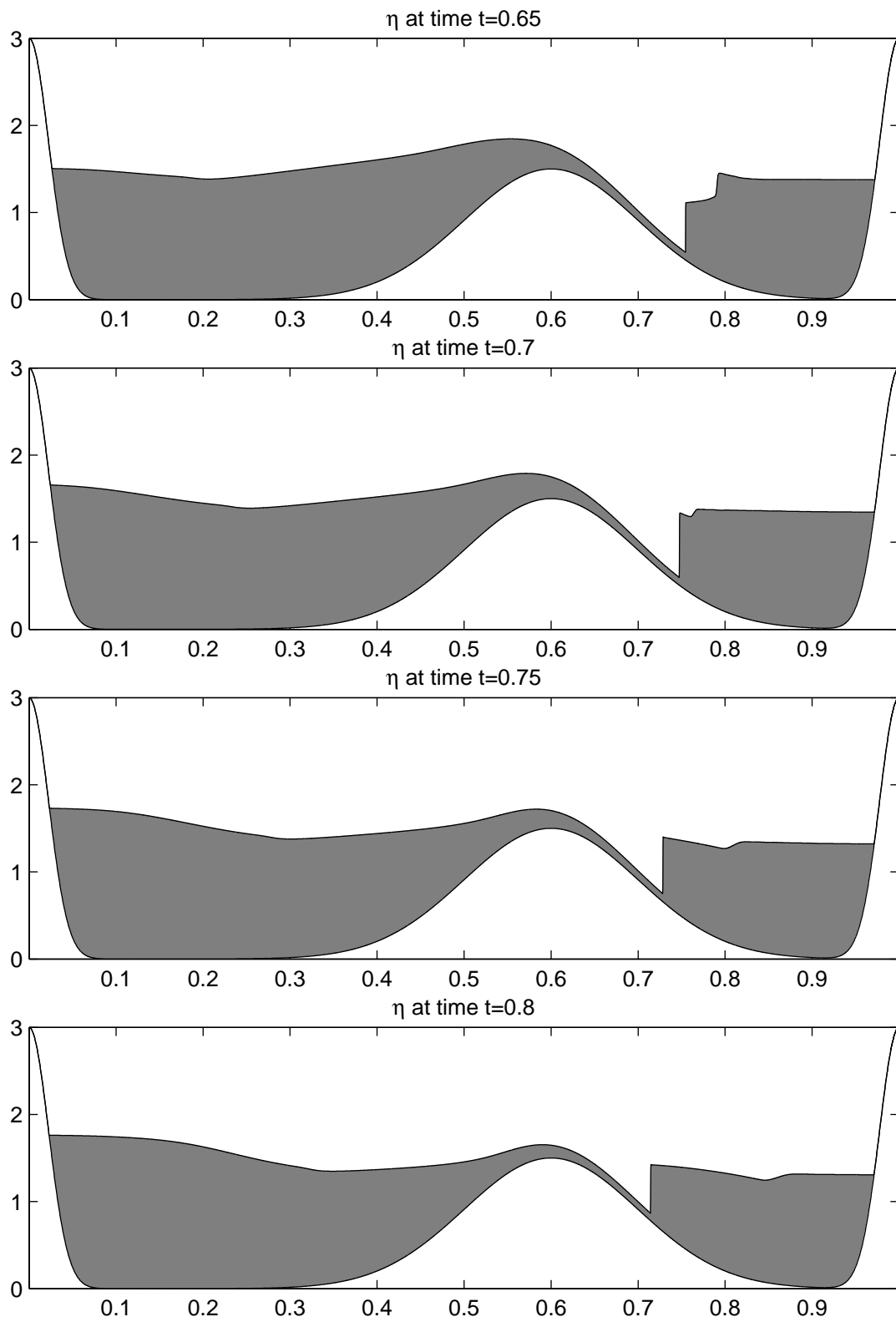
Figure 3.6 continued

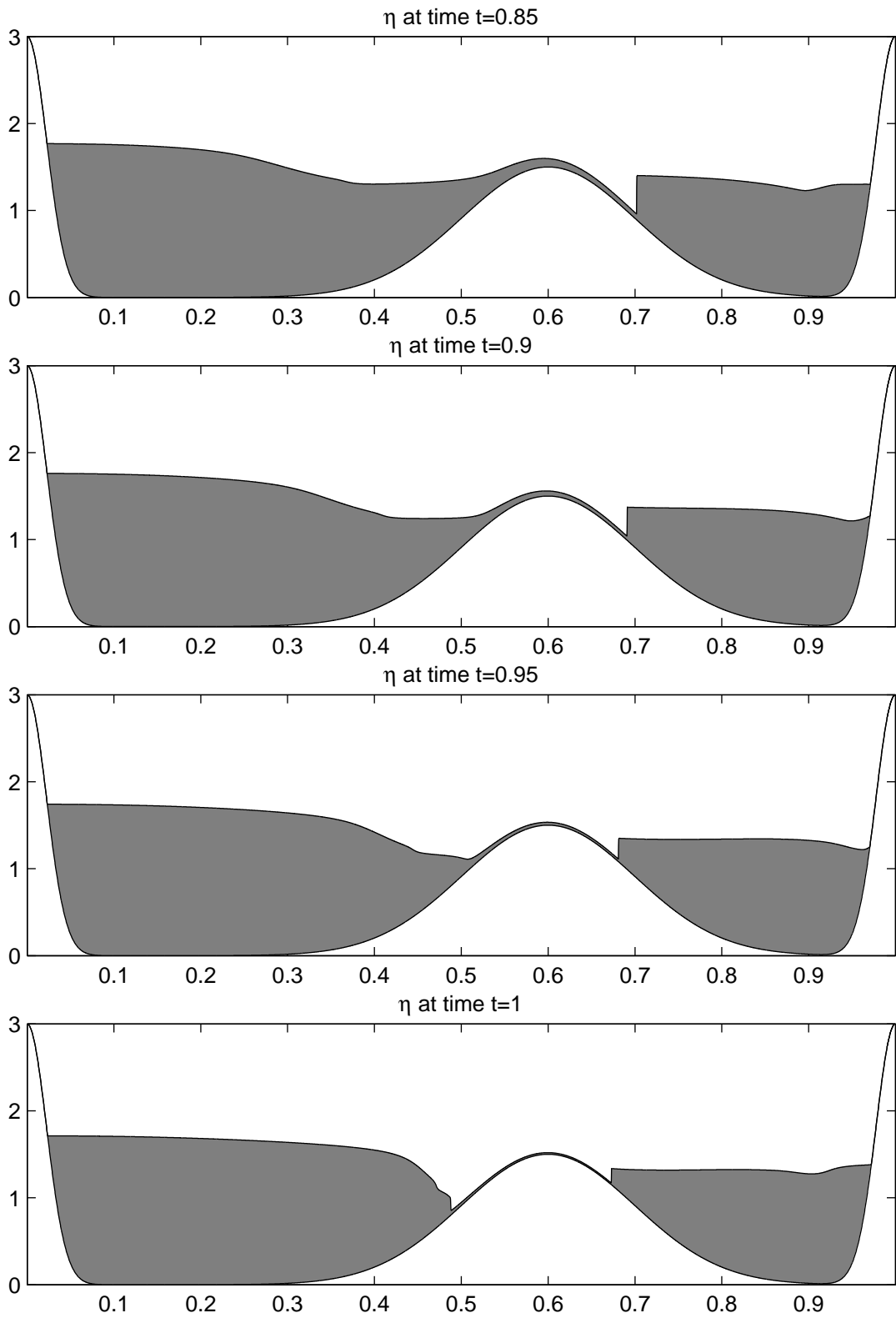Figure 3.6 continued

Figure 3.6 continued

Figure 3.6 continued

BIBLIOGRAPHY

[1] D. Bale, R. J. LeVeque, S. Mitran, and J. Rossmanith. A wave-propagation method for conservation laws or balance laws with spatially varying flux functions. *SIAM J. Sci. Comp.*, 24:266–278, 2002.

[2] T. Buffard, T. Gallouet, and J. M. Herard. A naïve Godunov scheme to solve the shallow water equations. *CR Acad Sci Paris*, 1(326):885–890, 1998.

[3] B. Carrier and H. Greenspan. Water waves of finite amplitude on a sloping beach. *Journal of Fluid Mech.*, 62:97–109, 1957.

[4] J. F. Colombeau. *Multiplication of Distributions: A tool in mathematics, numerical engineering and theoretical physics.* Springer—Verlag, Berlin, 1992.

[5] B. Einfeldt. On Godunov-type methods for gas dynamics. *SIAM J. Numer. Anal.*, 25:294–318, 1988.

[6] B. Einfeldt, C. D. Munz, P. L. Roe, and B. Sjogreen. On Godunov-type methods for near low densities. *J. Comput. Phys.*, 92:273–295, 1991.

[7] T. Gallouet and H. Jean-Marc. Some approximate Godunov schemes to compute shallow water equations with topography. *Computers and Fluids*, 32:479–513, 2003.

[8] E. Godlewski and P. A. Raviart. *Numerical Approximation of Hyperbolic Systems of Conservation Laws.* Springer, New York, 1996.

[9] J. M. Greenberg and A. Y. LeRoux. A well-balanced scheme for numerical processing of source terms in hyperbolic equations. *SIAM Journal of Numerical Analysis*, 33:1–16, 1996.

[10] A. Harten, P. D. Lax, and B. van Leer. On upstream differencing and Godunov-tpye schemes for hyperbolic conservation laws. *SIAM Review*, 25:235–61, 1983.

[11] T. Hou and P. LeFloch. Why non-conservative schemes converge to the wrong solutions: Error analysis. *Math. of Comput.*, 62:497–530, 1994.

[12] A. Kurganov and D. Levy. Central upwind schemes for the St. Venant system. *Mathematical Modelling and Numerical Analysis*, 36:397–425, 2002.

[13] R. J. LeVeque. CLAWPACK software. `http://www.amath.washington.edu/~claw`.

[14] R. J. LeVeque. Balancing source terms and flux gradients in high-resolution Godunov methods: The quasi-steady wave propagation algorithm. *Journal of Computational Physics*, 146:346–365, 1998.

[15] R. J. LeVeque. *Finite Volume Methods For Hyperbolic Problems*. Cambridge Texts in Applied Mathematics. Cambridge University Press, Cambridge, United Kingdom, 2002.

[16] J.J. Stoker. *Water Waves: The Mathematical Theory with Applications*. Interscience Publishers, New York, 1957.

[17] E. F. Toro. *Riemann Solvers and Numerical Methods for Fluid Dynamics*. Springer–Verlag, Berlin, 1997.

[18] E. F. Toro. *Shock Capturing Methods for Free Surface Shallow Flows*. John Wiley and Sons, Chichester,United Kingdom, 2001.

[19] G. Whitham. *Linear and Nonlinear Waves.* John Wiley and Sons, New York, 1974.